

## Revising the Spin and Kick Connection in Isolated Binary Black Holes

VISHAL BAIBHAV<sup>1,2,\*</sup> AND VICKY KALOGERA<sup>3,2,4</sup>

<sup>1</sup>*Columbia Astrophysics Laboratory, Columbia University, 550 West 120th Street, New York, NY 10027, USA*

<sup>2</sup>*Center for Interdisciplinary Exploration and Research in Astrophysics (CIERA), Northwestern University, 1800 Sherman Ave, Evanston, IL 60201, USA*

<sup>3</sup>*Department of Physics and Astronomy, Northwestern University, 2145 Sheridan Road, Evanston, IL 60208, USA*

<sup>4</sup>*NSF-Simons AI Institute for the Sky (SkAI), 172 E. Chestnut St., Chicago, IL 60611, USA*

(Dated: December 5, 2024)

### ABSTRACT

The origin of black hole (BH) spins remains one of the least understood aspects of BHs. Despite many uncertainties, it is commonly assumed that if BHs originated from isolated massive star binaries, their spins should be aligned with the orbital angular momentum of the binary system. This assumption stems from the notion that BHs inherit their spins from their progenitor stars. In this study, we relax this long-held viewpoint and explore various mechanisms that can spin up BHs before or during their formation. In addition to natal spins, we discuss physical processes that can spin BHs isotropically, parallel to natal kicks, and perpendicular to natal kicks. These different mechanisms leave behind distinct imprints on the observable distributions of spin magnitudes, spin-orbit misalignments and the effective inspiral spin of merging binaries. In particular, these mechanisms allow even the binaries originating in the field to exhibit precession and retrograde spin ( $\chi_{\text{eff}} < 0$ ). This broadens the parameter space allowed for isolated binary evolution into regimes which were previously thought to be exclusive to dynamically assembled binaries.

### 1. INTRODUCTION

One of the least understood aspects of compact objects is the origin of their spins, especially those of black holes (BHs). The most popular theory suggests that compact objects inherit their spin from their parent star's angular momentum, specifically from the collapsing iron core of the progenitor star (Heger et al. 2005; Ott et al. 2006). However, this theory is not fully supported by observations. The current understanding of the origin of compact object spins suggests that their natal spins, inherited from the parent star's angular momentum, are insufficient to explain the wide range of spins observed in BHs and pulsars (Kaspi & Helfand 2002; Faucher-Giguere & Kaspi 2006; Popov et al. 2011; Popov & Turolla 2012). Asteroseismic measurements point towards efficient angular momentum transport between the stellar core and envelopes, leading to slower rotation rates of the cores (e.g. Marques et al. (2013); Cantiello et al. (2014); Fuller & Ma (2019); Eggenberger et al. (2019); Takahashi &

Langer (2021)). This could imply that the spins of compact objects are not always inherited from their parent stars. In fact, stellar rotation is not the only possible source of angular momentum in compact objects. A range of mechanisms have been proposed, including inward transport of angular momentum through internal gravity waves during the progenitor evolution (Fuller et al. 2014, 2015; Ma & Fuller 2019; McNeill & Müller 2020), spin-up of the newly formed proto-neutron star during the pre-explosion phase by anisotropic accretion downflows (Wongwathanarat et al. 2013; Coleman & Burrows 2022; Burrows et al. 2023), spin-up by triaxial instabilities such as spiral modes of the stalled supernova shock (Blondin & Mezzacappa 2007; Fernandez 2010; Rantsiou et al. 2011; Guilet & Fernández 2014; Kazeroni et al. 2016; Moreno Méndez & Cantiello 2016; Kazeroni et al. 2017), or the accretion of angular momentum associated with turbulent mass motions in the infalling convective layers of the collapsing progenitor star (Gilkis & Soker 2014; Gilkis & Soker 2016; Quataert et al. 2019; Antoni & Quataert 2022, 2023).

The prevalent assumption is that the spin of compact objects is derived from the angular momentum of their

vb2630@columbia.edu

\* NASA Einstein Fellow

parent star. Since the spin of the star is typically aligned with the orbital angular momentum, it would follow that the spin of compact objects should also be preferentially aligned. However, this is inconsistent with observations of compact objects in the field, as their spins do not appear to be aligned. For instance, binary neutron star systems, where the young neutron star is visible as a radio pulsar, have been observed to be large misalignment angles:  $130.04 \pm 0.4^\circ$  for PSR J0737-3039B and  $104 \pm 9^\circ$  for PSR J1906+0746 (Breton et al. 2008; Desvignes et al. 2019). Furthermore, the X-ray binaries Cyg X-1 (Zdziarski et al. 2023), Cyg X-3 (Zdziarski et al. 2018) and MAXI J1820+070 (Poutanen et al. 2022) also exhibits large spin misalignments of  $20\text{-}30^\circ$ ,  $37^\circ$  and  $> 40^\circ$  respectively. These observations offer compelling evidence to indicate that compact objects do not inherit their spins from stars.

BHs and neutron stars (NSs) are born with natal kick velocities typically ranging from  $O(10 \text{ km/s})$  to  $O(100 \text{ km/s})$  (Mandel & Müller 2020; Igoshev et al. 2021; Stevenson 2022; O’Doherty et al. 2023; Kapil et al. 2023; Mandel & Igoshev 2023). This is supported by observed proper motions of young radio pulsars and by analyzing the orbital parameters and spin orientations of NSs in binary systems (Harrison et al. 1993; Lyne & Lorimer 1994; Kaspi et al. 1996; Fryer et al. 1998; Lai et al. 2001; Arzoumanian et al. 2002; Chatterjee et al. 2005; Hobbs et al. 2005). These natal kicks may be attributed to asymmetrical explosions or anisotropic emission of neutrinos that carry a significant amount of binding energy from the compact star. (Woosley 1987; Bisnovatyi-Kogan 1993; Janka & Mueller 1994; Burrows & Hayes 1996; Fryer & Kusenko 2006; Kusenko et al. 2008; Sagert & Schaffner-Bielich 2008).

Remarkably, radio observations of pulsars have shown that the spins of these rapidly rotating neutron stars often align with their proper motion (Johnston et al. 2005, 2007; Ng & Romani 2007; Noutsos et al. 2012). This alignment implies that there could be a close link between the physical processes that initiate the spin of a BH or neutron star, and those that cause the recoil during core-collapse (CC). The alignment between the spin and kick of neutron stars can arise from multiple factors, including spiral standing accretion shock instability (SASI) motions, large-scale velocity and density perturbations in convective burning shells, and dipolar neutrino-emission asymmetry associated with the lepton-number emission self-sustained asymmetry (LESA) phenomenon (Janka 2017). Moreover, the initial kick of the neutron star can cause it to be increasingly offset from the explosion center, leading to one-sided accretion of tangential vortex flows in the fallback matter, which could also contribute

to the alignment Janka et al. (2022). However, various mechanisms may cause the spin of compact objects to be perpendicular to their kicks, such as off-center explosions or asymmetric and partial fallback of ejecta (Spruit & Phinney 1998; Chan et al. 2020). In many CC simulations, spins and kicks are also found to be perpendicular (Chan et al. 2020; Powell & Müller 2020; Stockinger et al. 2020). In addition, during the course of binary evolution, the mass transfer can lead to a flip in the spin direction onto the orbital plane under certain conditions, resulting in a tilt angle of  $\pi/2$  relative to the orbital angular momentum (Matese & Whitmire 1983; Stegmann & Antonini 2021). In such cases, the distribution of resulting tilt angles exhibits a strong bimodal behavior, with the majority of spins either parallel or perpendicular to the orbital angular momentum. This misalignment, caused by mass transfer, can even override the effect of tidal synchronization, particularly during phases of rapid mass transfer (Stegmann & Antonini 2021). Tauris (2022) have also suggested that the BH spin axis may get tossed during the core collapse and might not be necessarily aligned with the orbital angular momentum (see also Farr et al. 2011, for NS spin tossing), potentially affecting the observed distribution of BBH mergers by LIGO-Virgo-KAGRA (LVK) Collaboration.

In this article, our aim is to explore how different mechanisms that can give BHs their spins impact the resulting spin magnitudes, spin-orbit tilts, and effective inspiral spins. We introduce the primary mathematical framework for accounting for spin-orbit tilts during CC in Section 2, which includes implementing four potential models for spin orientations: BH spin inherited from progenitor stars, isotropic BH spins, BHs spun up along the direction of their natal kicks, and BHs spun up perpendicular to the direction of their natal kicks. Subsequently, in Section 3, we apply these models to a population of merging BHs taking into account various factors, such as natal kicks, spin magnitudes, orbital separations, and tidal interactions. We analyze the impact of each spin model on GW observables like spin magnitudes, spin-orbit tilts, and effective inspiral spin parameters. Finally, we provide our conclusion in Section 4.

## 2. SPIN-ORBIT MISALIGNMENTS

We set up a reference frame to analyze the spin-orbit dynamics as illustrated in Fig. 1. We assume a binary star system on a circular orbit with mass  $M_i$ , initial separation  $a_i \hat{\mathbf{r}}$  and orbital angular momentum along  $\mathbf{L}_i$ . A CC causes one of the stars to receive a natal kick  $\mathbf{v}_k$ , where the kick direction is defined using two angles, namely the polar angle  $\theta_k$  and the azimuthal angle  $\phi_k$ . The polar angle  $\theta_k$  represents the angle between the kick

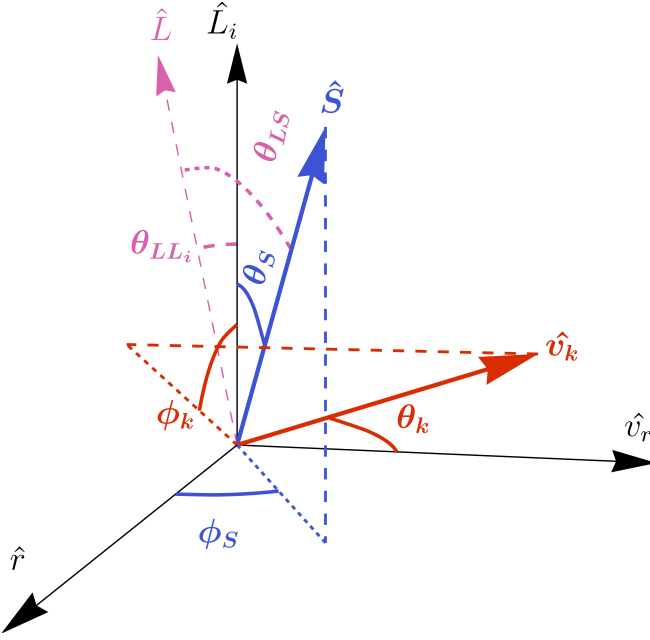


**Figure 1.** Angles involved in studying natal kicks. The binary system components are initially separated along the unit vector  $\hat{\mathbf{r}}$ , with a relative velocity of  $\mathbf{v}_0$ , before the CC. The BH progenitor has a spin given by  $(\theta_S, \phi_S)$  (highlighted in red) and receives a natal kick along the unit vector  $\hat{\mathbf{v}}_k$  given by angles  $(\theta_k, \phi_k)$  (highlighted in blue). Due to the natal kick, the orbital angular momentum tilts by an angle  $\theta_{LL_i}$  from the  $\mathbf{L}_i$  to  $\mathbf{L}$  (highlighted in pink). The change in the orbit tilt causes the spin-orbit misalignment to change from  $\theta_S$  to  $\theta_{LS}$ .

velocity vector  $\mathbf{v}_k$  and the pre-CC orbital velocity vector  $\mathbf{v}_0$ , and the azimuthal angle  $\phi_k$  is the angle subtended in the  $\mathbf{L}_i - \mathbf{r}$  plane, where  $\phi_k = 0$  implies kicks parallel to the initial angular momentum  $L_i$ .

The CC decreases the total mass of the binary system from  $M_i$  to  $M_f$  and alters the velocity of the exploding star from  $\mathbf{v}_0$  to  $\mathbf{v}_0 + \mathbf{v}_k$ . Applying energy and angular momentum conservation to the binary system before and after the CC, we can determine the final values of semi-major axis ( $a_f$ ) and eccentricity ( $e$ ) as follows (Brandt & Podsiadlowski 1995; Kalogera 1996, 2000):

$$\frac{a_f}{a_i} = \frac{\beta}{[2(\beta - 1) + 1 - u_k^2 - 2u_k \cos \theta_k]}, \quad (1)$$

$$1 - e^2 = \frac{2\beta - u_k^2 \sin^2 \theta_k - (u_k \cos \theta_k + 1)^2}{\beta^2} \times (u_k^2 \sin^2 \theta_k \cos^2 \phi_k + (1 + u_k \cos \theta_k)^2) \quad (2)$$

where  $\beta$  is the ratio of the final mass  $M_f$  to the initial mass  $M_i$ , and  $u_k$  is the the kick magnitude normalized to the circular orbital velocity before the explosion:

$$u_k = \frac{v_k}{v_0} = v_k \sqrt{\frac{a_i}{GM_i}}. \quad (3)$$

When  $e > 1$ , the CC will disrupt the binary system. This occurs when the kick velocity  $\mathbf{v}_k$  has a large component along the initial orbital velocity vector  $\mathbf{v}_0$ . The maximum value of  $\cos \theta_k$ , beyond which the binaries get disrupted, can be expressed as (Brandt & Podsiadlowski 1995; Kalogera 1996, 2000):

$$\cos \theta_k < \cos \theta_k^{\max} \equiv \frac{2\beta - u_k^2 - 1}{2u_k} \quad (4)$$

The probability of a binary not getting disrupted is  $(1 + \cos \theta_k^{\max})/2$ . It should be noted that binaries do not disrupt when  $u_k < \sqrt{2\beta} - 1$ , while all binaries will disrupt if  $u_k > \sqrt{2\beta} + 1$  (Brandt & Podsiadlowski 1995).

The binary separation due to a CC changes between (Brandt & Podsiadlowski 1995; Kalogera 1996, 2000)

$$\frac{a_f}{a_i} \in \left[ \frac{\beta}{2\beta - (1 - u_k)^2}, \infty \right) \quad (5)$$

The final separation is smallest when  $\mathbf{v}_0$  and  $\mathbf{v}_k$  are antiparallel ( $\cos \theta_k = -1$ ), while at  $\cos \theta_k = \cos \theta_k^{\max}$ , the binary disrupts, i.e.  $a_f = \infty$ . The minimum separation that can be reached is  $a_f = a_i/2$  when  $u_k = 1$ . The probability that the binary separation can shrink (but only when  $1 - \sqrt{\beta} < u_k < 1 + \sqrt{\beta}$ ) is

$$p(a_f < a_i) = \frac{\beta - (u_k - 1)^2}{4u_k} \quad (6)$$

This probability achieves a maximum value of  $(1 - \sqrt{1 - \beta})/2$  at  $u_k = \sqrt{1 - \beta}$ .

The CC also causes the orbital plane of the binary to tilt by an angle  $\theta_{LL_i}$  (Kalogera 2000),

$$\cos \theta_{LL_i} = \frac{u_k \cos \theta_k + 1}{\sqrt{u_k^2 \sin^2 \theta_k \cos^2 \phi_k + (u_k \cos \theta_k + 1)^2}} \quad (7)$$

In the case of low magnitude kicks, the orbital tilts are limited to small values (Kalogera 2000). As the natal kick magnitude increases, the range of allowed tilt angles in binary black hole (BBH) systems expands, and the peak of the angle distribution shifts towards higher values. However, when the kick magnitude becomes comparable to or slightly higher than the orbital velocity ( $u_k > 1$ ), the full range of tilt angles from alignment ( $\cos \theta_{LS} = 1$ ) to antialignment ( $\cos \theta_{LS} = -1$ ) with the orbital angular momentum axis becomes possible. When the kick magnitude is even higher than  $\sqrt{2\beta + 1}$ , the tilt

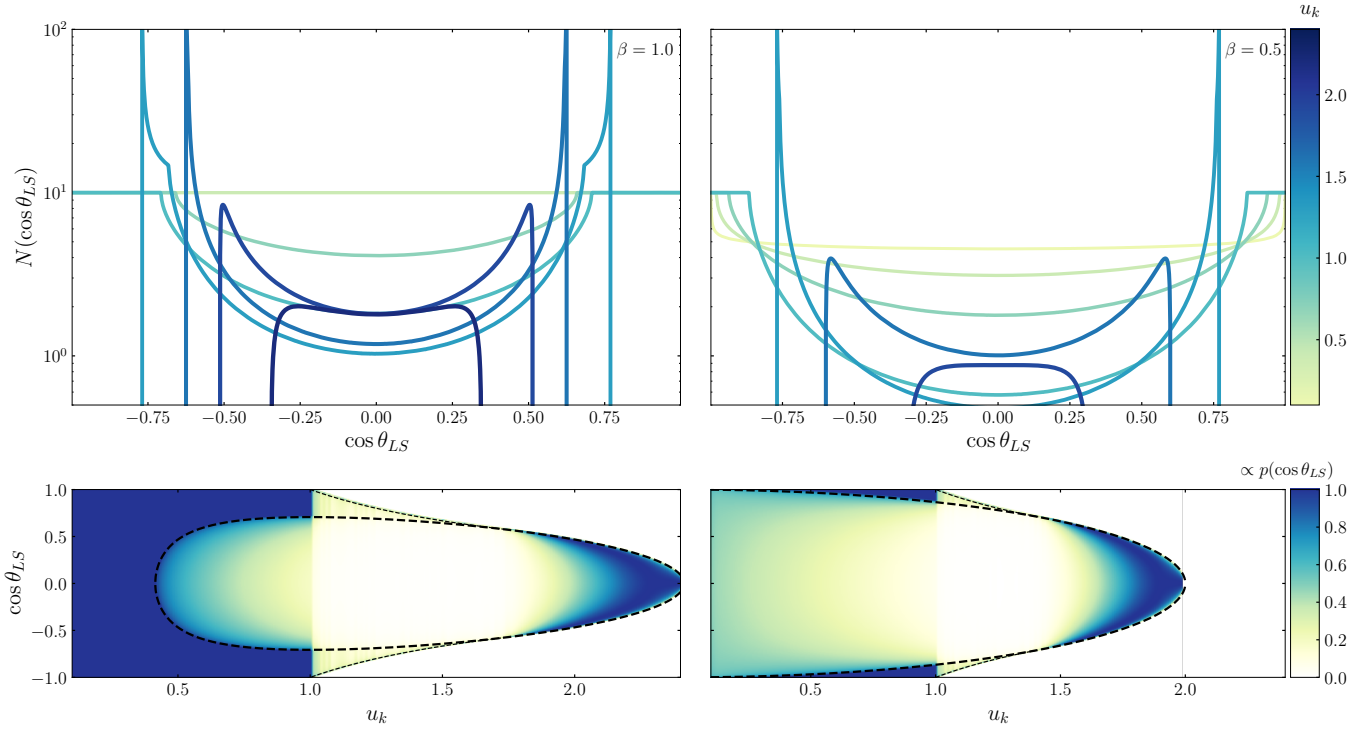


**Figure 2.** Distributions of  $\cos\theta_{LS}$  for Par models. Top panels: Histograms  $N(\cos\theta_{LS})$  of the spin-orbit misalignment angle  $\cos\theta_{LS}$  for different values of  $u_k$ , ranging from 0.1 (light green) to 2.2 (dark blue) in increments of 0.3, for  $\beta = 1$  (left) and  $\beta = 0.5$  (right). Lower panels: probability density functions of  $\cos\theta_{LS}$ , normalized by the maximum value, as a function of  $u_k$  and  $\cos\theta_{LS}$ . The dashed lines correspond to Eq. (12), and the dotted lines mark the position of the peaks at  $1/u_k$ .

angles exceed  $90^\circ$ , leading to retrograde post-CC orbits. The allowed ranges for spin-orbit misalignment for a given  $u_k$  is

$$\cos\theta_{LL_i} \in \begin{cases} (\sqrt{1-u_k^2}, 1] & u_k < 1 \\ [-1, 1] & 1 \leq u_k < \sqrt{2\beta+1} \\ \left[-1, \frac{1-u_k^2+2\beta}{\sqrt{8\beta}}\right] & \sqrt{2\beta+1} \leq u_k < \sqrt{2\beta}+1 \\ \text{disrupted} & u_k \geq \sqrt{2\beta}+1. \end{cases} \quad (8)$$

The direction of the spin vector  $\mathbf{S}$  of the collapsing star can be specified by two angles, namely the angle  $\theta_S$  between the spin vector  $\mathbf{S}$  and the orbital angular momentum vector  $\mathbf{L}_i$ , and the angle  $\phi_S$  between the projection of the spin vector  $\mathbf{S}$  onto the orbital plane and the separation vector  $\hat{\mathbf{r}}$  between the binary members. The CC causes the angle between the binary's spin vector  $\mathbf{S}$  and its orbital angular momentum vector  $\mathbf{L}$  to change from  $\theta_S$  to  $\theta_{LS}$ , where:

$$\cos\theta_{LS} = \cos\theta_S \cos\theta_{LL_i} + \sin\theta_S \sin\theta_{LL_i} \sin\phi_S \quad (9)$$

Our goal is to understand how different physical mechanisms that impart spins to BHs also impact post-CC spin-orbit misalignment. Each of these mechanisms generates distinct descriptions of the BH spin direction, represented by  $(\theta_S, \phi_S)$ , which will have varying effects on the distributions of  $\theta_{LS}$ . Next, we explore four potential scenarios of spin angles and analyze how they shape the distributions of  $\theta_{LS}$  and study how these mechanisms can be observed through the unique signatures they leave on the population of BH mergers.

### 2.1. Natal spins

Most binary star systems display spins aligned with orbital angular momentum.<sup>1</sup> This alignment is often anticipated given both stars originate from the same portion of a molecular cloud. If the angular momentum of a star is preserved during its collapse into a BH, the resulting BH should also have spin aligned with the

<sup>1</sup> Note that binary stars with perfectly aligned spins are not always the norm, as demonstrated by the BANANA (Binaries Are Not Always Neatly Aligned) project. This project conducted measurements of spin-orbit misalignments in close binary star systems, revealing many notable exceptions to the spin alignment of binary stars (Albrecht et al. 2007, 2009, 2011, 2013, 2014; Marcussen & Albrecht 2022; Marcussen et al. 2024).

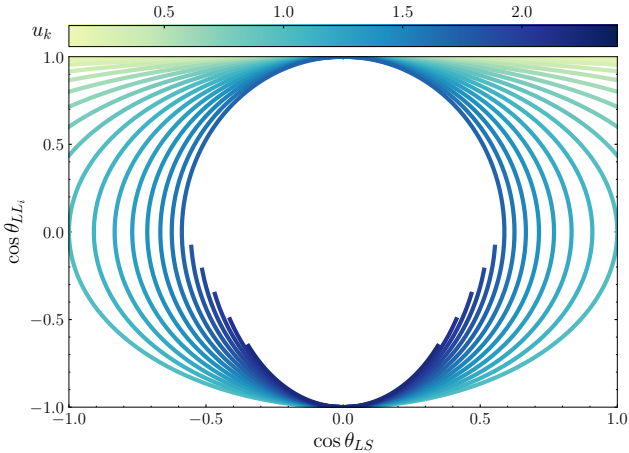


**Figure 3.** Relation between  $\cos\theta_{LS}$  and  $\cos\theta_{LL_i}$  for Par model following Eq. (14) assuming  $\beta = 1$  for  $u_k$  ranging from 0.1 to 2.2 in increments of 0.1 and orbital tilts given by Eq. (8).

orbital angular momentum. However, the collapsing star can impart linear momentum recoils onto the newly-formed BH, causing spin-orbit misalignment in the BBH system. The distribution of spin-orbit misalignment has been extensively explored in Fragos et al. (2010); Rodriguez et al. (2016); O’Shaughnessy et al. (2017); Rodriguez & Antonini (2018); Wysocki et al. (2018); Atri et al. (2019); Salvesen & Pokawanvit (2020); Zhu (2021); Callister et al. (2021); Steinle & Kesden (2021, 2022); Gompertz et al. (2022). If the spin vector  $\mathbf{S}$  is aligned with  $\mathbf{L}$  before the CC ( $\theta_S = 0$ ), the tilt of the orbital plane equals the misalignment of the exploding star’s spin ( $\theta_{LS} = \theta_{LL_i}$ ). From now on, we will refer to the model that assumes BHs inherit their spin from their parent stars as **Natal**.

### 2.2. Isotropic spins

BHs may not necessarily inherit their spin from their parent star. Instead, they may acquire their spin through various mechanisms that could impart a spin in a random direction. Several such mechanisms have been proposed in the literature. For example, Fuller et al. (2014, 2015); Ma & Fuller (2019); McNeill & Müller (2020) suggested that internal gravity waves excited during late-time burning phases or envelope convection could spin up non-rotating CC progenitors. This stochastic spin-up leads to a Maxwellian distribution of pre-collapse core spin magnitudes and isotropic spin directions that are unrelated to the envelope’s spin. Another possibility is that during a massive star’s collapse without an energetic explosion, some of its hydrogen envelope may fall onto the newborn BH. The infalling convective shells in the star have random velocity fields that result in a finite

angular momentum at each shell (Gilkis & Soker 2014; Gilkis & Soker 2016; Quataert et al. 2019; Antoni & Quataert 2022, 2023). The accretion of this convective envelope can cause the BH to spin (with a final spin parameter of up to 0.8), despite the progenitor star not rotating. In core collapse simulations, transfer of angular momentum to the NS can also happen via stochastic accretion downflows during the post-bounce accretion phase, leading to the random orientation of neutron star (NS) spins (Wongwathanarat et al. 2013).

Henceforth, we will use the term **Iso** to describe the model that assumes BHs are spun up in isotropic directions and hence  $\cos\theta_{LS}$  is uniformly distributed in  $[-1, 1]$ .

### 2.3. BH spins parallel to natal kicks

Observational evidence indicates that there is typically an alignment between the spin and proper motion in young pulsars (Kramer et al. 2003; Johnston et al. 2005; Wang et al. 2006; Ng et al. 2006; Johnston et al. 2007; Chatterjee et al. 2009; Noutsos et al. 2012; Noutsos et al. 2013; Mandel & Igoshev 2023). Since most observations can only measure the transverse velocity of pulsars, the alignment between the natal kicks and spin direction is inferred in a two-dimensional projection on the plane of the sky. However, recent observations using the Five-hundred-meter Aperture Spherical radio Telescope (FAST) have shown that PSR J0538+2817 has almost perfect 3D alignment between its spin axis and velocity vector to within approximately  $6^\circ$  (Yao et al. 2021). Janka (2017) proposed three ways that can lead to this spin-kick alignment in neutron stars: spiral SASI motions, large-scale velocity and density perturbations in convective burning shells, and dipolar neutrino-emission asymmetry associated with the LESA phenomenon. According to Janka et al. (2022), the natal kick causes the neutron star to be increasingly offset from the explosion center, leading to one-sided accretion of tangential vortex flows in the fallback matter, ultimately leading to spin-kick alignment (see Müller 2023, for counter-argument). In simulations by Müller et al. (2017), the proto-neutron star, which initially gained angular momentum in a direction perpendicular to the kick after shock revival, shows a trend towards spin-kick alignment as the angle between the spin axis and kick decreases from  $80^\circ$  to  $40^\circ$ . Although longer simulations are required to confirm whether this trend continues towards even smaller misalignment, the observed trend suggests the possible existence of a systematic alignment mechanism. CC simulations by Burrows et al. (2024) also discovered a potential correlation or anti-correlation between the spin and natal kicks of compact objects. They observed that

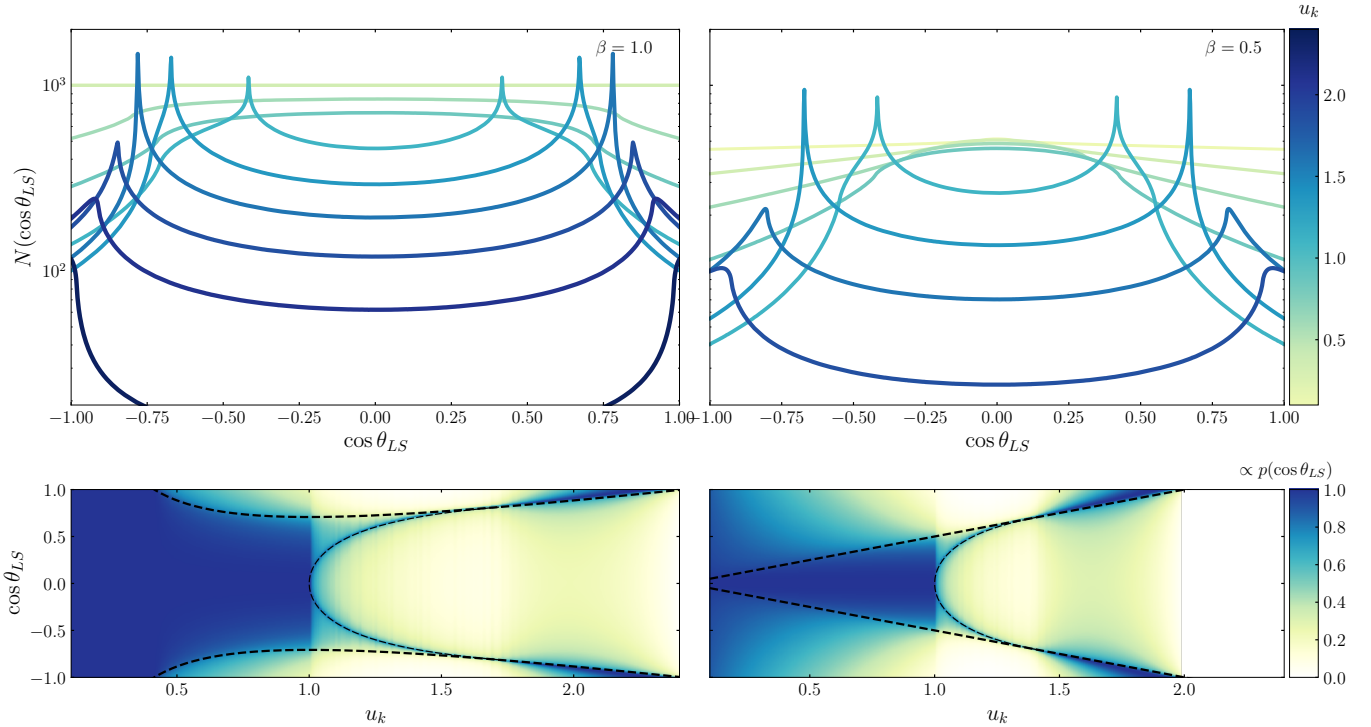


**Figure 4.** Distributions of  $\cos\theta_{LS}$  for **Perp** models. Top panels: Histograms  $N(\cos\theta_{LS})$  of the spin-orbit misalignment angle  $\cos\theta_{LS}$  for different values of  $u_k$ , ranging from 0.1 (light green) to 2.2 (dark blue) in increments of 0.3, for  $\beta = 1$  (left) and  $\beta = 0.5$  (right). Lower panels: probability density functions of  $\cos\theta_{LS}$ , normalized by the maximum value, as a function of  $u_k$  and  $\cos\theta_{LS}$ . The dashed lines correspond to Eq. (18), and the dotted lines mark the position of the peaks at  $\sqrt{u_k^2 - 1}/u_k$ .

the explosion and accretion tend to occur roughly perpendicular to each other, with accretion spinning up the periphery of the proto-neutron star. Consequently, the net spin vector aligns either parallel or anti-parallel to the kick direction.

Most population synthesis studies model the spin-kick alignment by assuming the spin axis to be the preferred direction with which the kick is aligned, based on the assumption that spins are inherited from the star and aligned with the orbital angular momentum, and natal kicks are drawn along this spin axis [Kalogera \(2000\)](#); [Willems et al. \(2004, 2005b\)](#); [Gerosa et al. \(2013\)](#); [Callister et al. \(2021\)](#); [Gompertz et al. \(2022\)](#). However, here we reverse this causal relation and assume that the natal kick defines the preferred direction along which spin is oriented. In this scenario, we assume that the kick is isotropic, and the compact object gets spun up parallel to the kick through one of the mechanisms mentioned above. We will use the term **Par** to describe the model that assumes BHs are spun up in the same direction as natal kicks, from now on.

In this case  $\mathbf{S} \parallel \mathbf{v}_k$ , angle subtended by the spin with the initial orbital angular momentum is

$$\cos\theta_S = \sin\theta_k \cos\phi_k$$

$$\sin\phi_S = \frac{\cos\theta_k}{\sqrt{(\sin\theta_k \sin\phi_k)^2 + \cos^2\theta_k}} \quad (10)$$

or using Eq. (9), the tilt angle between final orbital angular momentum and spin would be

$$\cos\theta_{LS} = \frac{\sin\theta_k \cos\phi_k}{\sqrt{u_k^2 \sin^2\theta_k \cos^2\phi_k + (u_k \cos\theta_k + 1)^2}} \quad (11)$$

To investigate the distribution of spin-orbit misalignment, we conduct Monte Carlo experiments involving  $10^6$  binaries, where we vary the value of  $u_k$  from 0 to  $\sqrt{2\beta + 1}$ . We assume two extreme mass loss scenarios, namely  $\beta = 0.5$  and  $\beta = 1$ . Additionally, we assume that the natal kicks have isotropic directions, which we sample uniformly in  $\cos\theta_k$  and  $\phi_k$ .

The outcomes of the Monte Carlo experiments are illustrated in Fig. 2. The top panels of the figure show the histograms for  $\cos\theta_{LS}$  for  $u_k$  ranging from 0.1 (light green) to 2.2 (dark blue) in increments of 0.3 for  $\beta = 1$  (left panel) and  $\beta = 0.5$  (right panels). In the lower panel, we plot the probability density functions of  $\cos\theta_{LS}$  as a function of  $u_k$ . We normalize these probability density functions such that the maximum value is 1. We expect that since the kick directions are isotropic and the spins are parallel to the kicks, the spins would

also be isotropic. However, not all kick directions are allowed as they disrupt the binary. This effect is reflected in the distributions in Fig. 2. For  $u_k < \sqrt{2\beta} - 1$ , no binary is disrupted, and therefore, the distribution of spin-orbit tilts is isotropic. However, at  $u_k > \sqrt{2\beta} - 1$ , the binaries begin to get disrupted, particularly if they have a large kick contribution along the orbital velocities ( $\cos \theta_k > \cos \theta_k^{\max}$ ). This effect impedes binaries from having large in-plane spins. For  $\sqrt{2\beta} - 1 < u_k < 1$ , there is a reduced number of systems with tilts in the range

$$|\cos \theta_{LS}| < \sqrt{\frac{1}{8\beta} \left( 4\beta - u_k^2 + 2 - \frac{(1 - 2\beta)^2}{u_k^2} \right)} \quad (12)$$

In Fig. 2, for  $u_k > 1$ , we observe interesting features. Specifically,  $\cos \theta_{LS}$  is bounded between

$$-\frac{1}{u_k} \leq \cos \theta_{LS} \leq \frac{1}{u_k}, \quad (13)$$

with the upper and lower bounds occurring at  $\cos \theta_k = -1/u_k$  and  $\cos \theta_{LL_i} = 0$ . We see very sharp peaks in the distribution at these extrema. Moreover, for  $u_k > \sqrt{2\beta} - 1$ , we observe an enhanced number of systems with spin-orbit tilts in the region given by Eq. (12). This reversal in trend can be understood by considering the absence of systems with spins in the pre-CC orbital plane. For  $u_k < 1$ , the angular momentum tilts are small, so the change in pre-CC and post-CC planes are also small. Therefore, there is a lack of systems with spins in post-CC planes. On the other hand, for  $u_k > \sqrt{2\beta} + 1$ , the orbit tilts by at least  $90^\circ$  (see Eq. (8)). Consequently, the spins that were previously in-plane and disfavored are now parallel to the angular orbital momentum. Similarly, spins that were initially aligned with the orbital angular momentum and favored are now in-plane post-CC tilt.

An alternative way to understand some of these features is by examining the relationship between  $\cos \theta_{LS}$  and  $\cos \theta_{LL_i}$ :

$$(u_k \cos \theta_{LS})^2 + (\cos \theta_{LL_i})^2 = 1. \quad (14)$$

We also plot this relation in Fig. 3 assuming  $\beta = 1$  for a range of  $u_k$  from 0.1 (yellow) to 2.2 (blue). The allowed range of  $\cos \theta_{LL_i}$  depends on the values of  $u_k$  and  $\beta$  according to Eq. (8), thereby also restricting the possible values of  $\cos \theta_{LS}$ . When  $u_k < 1$ ,  $\cos \theta_{LL_i}$  is positive, i.e. orbit can not tilt more than  $90^\circ$ , therefore  $\cos \theta_{LS}$  can also assume any value between  $[-1, 1]$ . As  $u_k$  increases beyond 1, the maximum value of  $|\cos \theta_{LS}|$  decreases to  $1/u_k$ . However, for  $u_k > \sqrt{2\beta} + 1$ , the tilt of the orbit is more than  $90^\circ$ , and the minimum value of  $\cos \theta_{LL_i}$  is given by Equation 8. This further restricts the allowed values of  $\cos \theta_{LS}$  according to Equation (14).

To summarize, in the model **Par** where BHs receive their spins parallel to the kicks, there are several important features of spin-orbit misalignment, including:

- For  $u_k < \sqrt{2\beta} - 1$ , the spin-orbit misalignments are isotropic.
- For  $\sqrt{2\beta} - 1 < u_k < \sqrt{2\beta} + 1$ , there are reduced number of systems with the spin-orbit misalignment given by Eq. (12).
- For  $u_k > 1$ , sharp peaks appear at the extrema of  $\cos \theta_{LS} = \pm 1/u$ .
- For  $u_k > \sqrt{2\beta} + 1$ , all the tilts are in the region given by Eq. (12)

#### 2.4. BH spins perpendicular to natal kicks

Although pulsar observations have shown spin-kick alignment, and various studies proposed hydrodynamical mechanisms claim to explain it, most 3D core collapse simulations show no indication of spin-kick alignment Wongwathanarat et al. (2013); Gessner & Janka (2018); Chan et al. (2020); Stockinger et al. (2020); Powell & Müller (2020), with an exception of Burrows et al. (2024) finding indications of alignment. Instead, Chan et al. (2020) showed that an asymmetric explosion with anisotropic and partial fallback can result in a BH spin of approximately 0.25, with the kick and spin vectors perpendicular to each other (cf. Fig. 10 in Chan et al. (2020)). Similar trends were identified by Stockinger et al. (2020) with perpendicular kick and spin, while Powell & Müller (2020) found a large angle of  $70^\circ$  between the two vectors. Spruit & Phinney (1998) have also suggested an off-center-kick scenario where the remnant receives a momentum impulse  $\mathbf{v}_k$  that is misaligned with the center of mass by  $\mathbf{r}_{\text{offset}}$ , resulting in the spin vector being perpendicular to the kick ( $\mathbf{r}_{\text{offset}} \times \mathbf{v}_k$ ). Farr et al. (2011) used off-center kicks to explain the large misalignments between spin and the orbital angular momentum of the binary pulsar PSR J0737-3039. Fragione & Loeb (2023) studied the population-level impact of off-center kicks on neutron star birth and constrained their offset locations using current Galactic pulsar observations. Such off-center explosions can be explained when the explosion is launched out of a SASI-active phase (Blondin & Mezzacappa 2007; Fernandez 2010; Guilet & Fernández 2014; Kazeroni et al. 2016, 2017), as observed by Janka (2017). Müller (2023) demonstrated that one-sided fallback accretion onto a compact object could also significantly contribute angular momentum perpendicular to the kick velocity. Henceforth, we will use the term **Perp** to denote the model that assumes BHs are spun up perpendicular to natal kick.

Given a natal kick  $\hat{\mathbf{v}}_{\mathbf{k}}$ , let us define the spin plane by two unit vectors as  $\mathbf{e}_1 = \sin \phi_k \hat{\mathbf{L}} - \cos \phi_k \hat{\mathbf{r}}$  (such that  $\mathbf{e}_1 \cdot \hat{\mathbf{v}}_{\mathbf{k}} = 0$ ) and  $\mathbf{e}_2 = \hat{\mathbf{v}}_{\mathbf{k}} \times \mathbf{e}_1$ . We can then define the spin direction as

$$\hat{\mathbf{S}} = \sin \phi_r \mathbf{e}_1 + \cos \phi_r \mathbf{e}_2 \quad (15)$$

Thus,  $\hat{\mathbf{S}}$  is given by three angles:  $\phi_k$  and  $\theta_k$  that decide the normal vector  $\hat{\mathbf{v}}_{\mathbf{k}}$  to the spin plane, while  $\phi_r$  decides the orientation of the spin in this plane. The angle subtended by the spin with the initial orbital angular momentum is given by

$$\cos \theta_S = \cos \theta_k \cos \phi_r \cos \phi_k + \sin \phi_r \sin \phi_k$$

$$\sin \phi_S =$$

$$\frac{-\sin \theta_k \cos \phi_r}{\sqrt{(\cos \theta_k \cos \phi_r \sin \phi_k - \sin \phi_r \cos \phi_k)^2 + (\sin \theta_k \cos \phi_r)^2}} \quad (16)$$

or using Eq. (9), the tilt angle between final orbital angular momentum and spin would be

$$\cos \theta_{LS} = \frac{\sin \theta_k \cos \phi_k}{\sqrt{u_k^2 \sin^2 \theta_k \cos^2 \phi_k + (u_k \cos \theta_k + 1)^2}} \quad (17)$$

To explore the distribution of spin-orbit misalignment, we perform Monte Carlo experiments by randomly sampling  $10^6$  binaries with uniform values of  $\cos \theta_k$ ,  $\phi_k$ , and  $\phi_r$ . We vary the value of  $u_k$  from 0 to  $\sqrt{2\beta} + 1$  while considering two extreme mass loss scenarios:  $\beta = 0.5$  and  $\beta = 1$ .

The results of our experiments are presented in Fig. 4. The top panels of the figure show histograms of  $\cos \theta_{LS}$  for  $u_k$  ranging from 0.1 (light green) to 2.2 (dark blue) in increments of 0.3 for  $\beta = 1$  (left panel) and  $\beta = 0.5$  (right panels). In the lower panel, we plot the probability density functions of  $\cos \theta_{LS}$ , normalized such that the maximum value is 1, as a function of  $u_k$ .

When  $u_k < \sqrt{2\beta} - 1$ , no binary is disrupted, and therefore, the distribution of spin-orbit tilts is isotropic. However, at  $u_k > \sqrt{2\beta} - 1$ , binaries begin to get disrupted, especially if they have a large kick contribution along the orbital velocities ( $\cos \theta_k > \cos \theta_k^{\max}$ ). This effect impedes binaries from having spins aligned with the orbital angular momentum. For  $\sqrt{2\beta} - 1 < u_k < 1$ , there is a reduced number of systems with tilts in the range

$$|\cos \theta_{LS}| > \frac{2\beta + u_k^2 - 1}{u_k \sqrt{8\beta}} \quad (18)$$

In Fig. 4, we observe interesting features for  $u_k > 1$ . Specifically, the distribution of  $\cos \theta_{LS}$  has sharp peaks at

$$\cos \theta_{LS} = \pm \frac{\sqrt{u_k^2 - 1}}{u_k}, \quad (19)$$

corresponding to  $\cos \theta_k = -1/u_k$  and  $\phi_r = \phi_k = 0$ . Additionally, for  $u_k > \sqrt{2\beta} - 1$ , there is an increase in the number of systems with tilts given by Eq. (12). This reversal in trend compared to behavior at  $u_k < 1$  can be understood by considering the absence of systems with spins aligned with the initial orbital angular momentum. For  $u_k < 1$ , the angular momentum tilts are small, resulting in a lack of systems with aligned spins. However, for  $u_k > \sqrt{2\beta} + 1$ , the orbit tilts by at least  $90^\circ$  (as shown in Eq. (8)). Consequently, the spins that were previously aligned with  $\mathbf{L}_i$  and disfavored are now perpendicular to  $\mathbf{L}$ . To summarize, in the model **Perp** where BHs receive their spins perpendicular to the kicks, there are several important features of spin-orbit misalignment, including:

- For  $u_k < \sqrt{2\beta} - 1$ , the spin-orbit misalignments are isotropic.
- For  $\sqrt{2\beta} - 1 < u_k < \sqrt{2\beta} + 1$ , there are reduced number of systems with the spin-orbit misalignment given by Eq. (18).
- For  $u_k > 1$ , sharp peaks appear at the extrema of  $\cos \theta_{LS} = \pm \sqrt{u_k^2 - 1}/u_k$ .
- For  $u_k > \sqrt{2\beta} + 1$ , tilt distributions are concentrated in the region given by Eq. (18)

### 3. POPULATION PROPERTIES OF MERGING BLACK HOLES

In this section, we generate Monte Carlo populations of BBHs under the four spin direction scenarios discussed here. Our primary objective is to investigate the implications of underlying mechanisms driving the BH spins on the population properties observed by LIGO-Virgo-KAGRA (LVK). By exploring the various imprints on the synthetic population, we aim to understand the physical processes responsible for shaping the observed properties of BBH populations detected through gravitational waves.

#### 3.1. Population model

Our synthetic simulations model the evolution of a binary system comprising two stars with masses  $M_1$  and  $M_2$  initially separated by  $a_{i1}$ . After the first CC event (CC1), the star with mass  $M_1$  transforms into a BH with mass  $m_1$ . Due to asymmetric ejecta, the BH experiences a recoil velocity  $v_{k1}$  changing the semimajor axis to  $a_{f1}$ . At a later stage in the binary's evolution, when the separation is  $a_{i2}$ , the secondary star with mass  $M_2$  undergoes CC (CC2), producing a BH with mass  $m_2$ . This event leads to mass loss and a recoil velocity  $v_{k2}$ , changing the binary's semimajor axis to  $a_{f2}$ . Next,

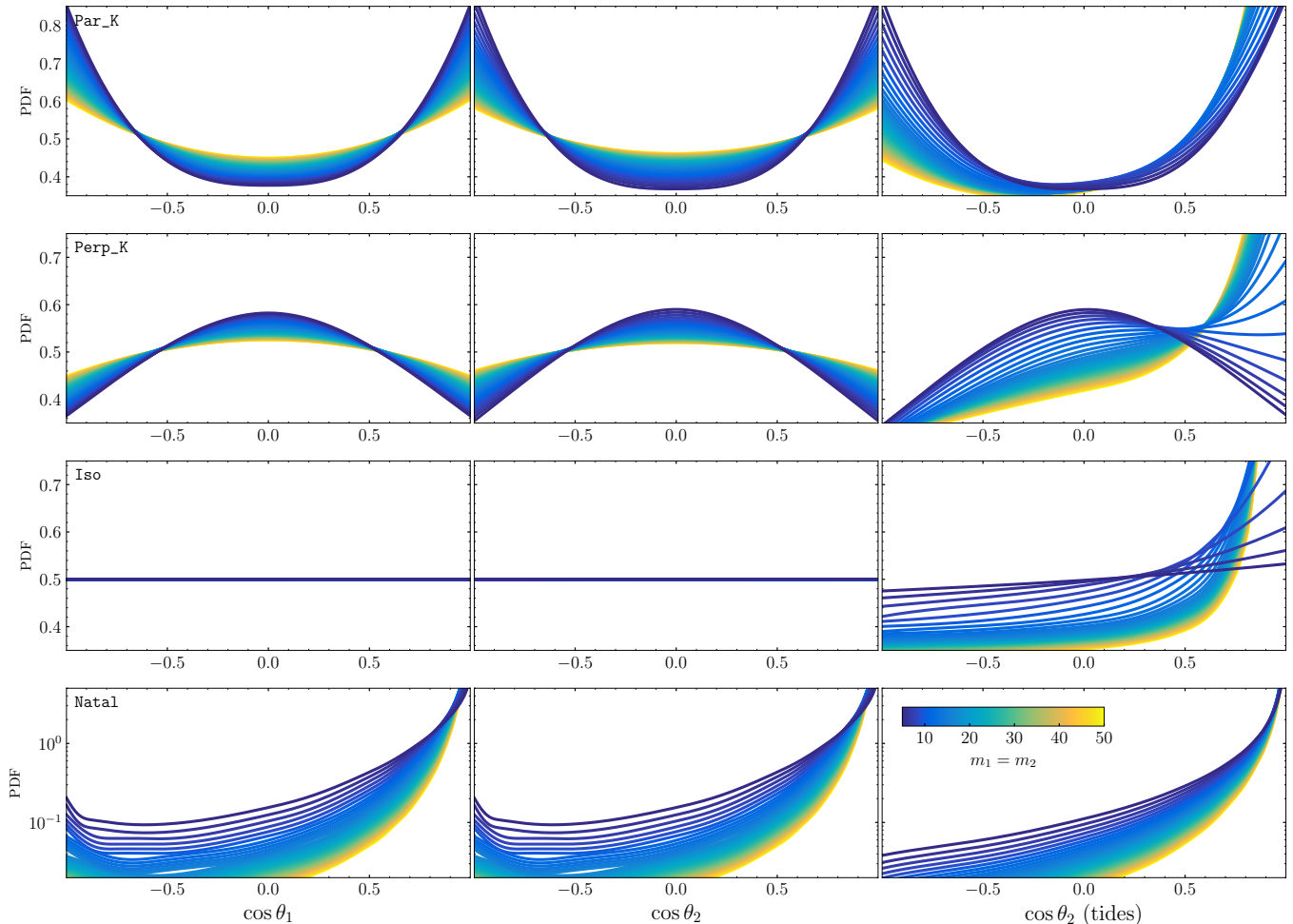


**Figure 5.** PDFs of spin-orbit tilts based on the non-interacting model for pre-CC2 orbital separations and high kicks for all BH masses:  $p(\cos \theta_1)$  (left),  $p(\cos \theta_2)$  assuming inefficient tides (middle), and  $p(\cos \theta_2)$  with tidal spin up (right) for the **Par**, **Perp**, **Iso**, and **Natal** models (from top to bottom) for BH masses ranging from  $m_1 = m_2 = 5M_\odot$  (in blue) to  $50M_\odot$  (in yellow).

we will elaborate on the prescriptions we use for orbital separations, natal kick magnitudes, spin magnitudes, and tidal interactions.

### 3.1.1. Semimajor axis

We begin by sampling the initial binary separation,  $a_{i1}$ , from a uniform logarithmic distribution in the range  $[10R_\odot, 10^4R_\odot]$ . Following the occurrence of CC1, the orbital separation changes to  $a_{f1}$  [Eq. (1)], and CC2, takes place at a distance  $a_{i2}$ . Our goal is to understand how different distributions of  $a_{i2}$  affect the population properties, and we consider two extreme scenarios :

**Non-interacting:** We assume that  $a_{f1} = a_{i2}$ , implying that the separation after CC1 and between CC2 remains unchanged. The evolution of the orbital separation is entirely governed by the natal kicks before the gravitational waves take over, driving the inspiral and reducing the separation until the BHs merge. However, in our synthetic population, a significant proportion of binaries

fail to merge within the Hubble time due to the broad range of initial orbital separations sampled.

**Interacting:** In reality, several physical processes such as stable mass transfer or common envelope can modify the binary separation between CC1 and CC2. Many binaries in various population synthesis models undergo at least one of these processes, leading to a significant reduction in orbital separation such that the BHs are close enough to merge via gravitational waves. While the full population synthesis is out of scope of this paper, we account for their effects by assuming that the separation changes from  $a_{f1}$  to  $a_{i2}$  in such a way that after CC2, when the separation again changes to  $a_{f2}$ , it is small enough to allow a merger within the Hubble time assuming zero eccentricity. This implies that all binaries that survived disruption during CC1 will merge after CC2.

### 3.1.2. Natal kick magnitudes

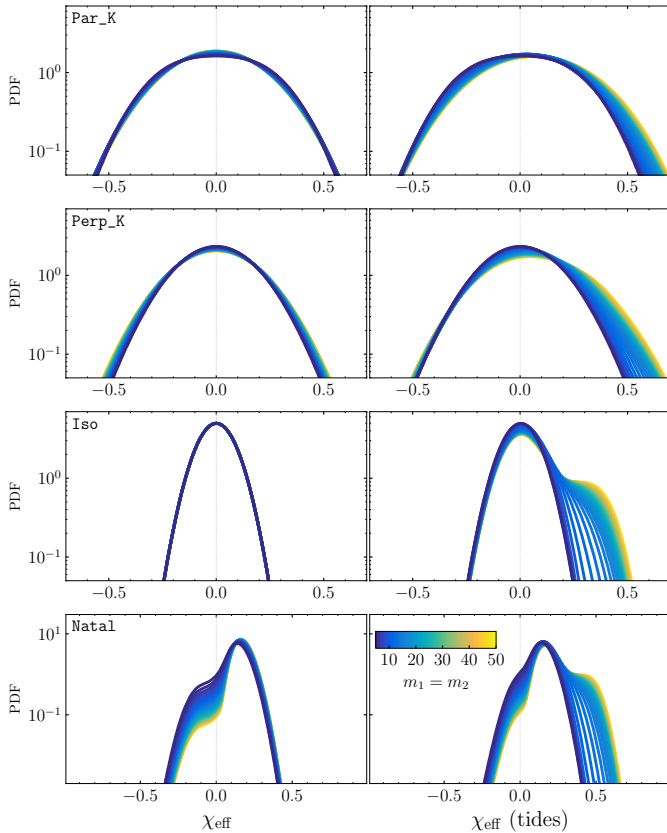


**Figure 6.** PDFs of  $\chi_{\text{eff}}$  based on the non-interacting model for pre-CC2 orbital separations and high kicks for all BH masses:  $p(\chi_{\text{eff}})$  assuming inefficient tides (left), and  $p(\chi_{\text{eff}})$  with tidal spin up (right) for the **Par**, **Perp**, **Iso**, and **Natal** models (from top to bottom) for BH masses ranging from  $m_1 = m_2 = 5M_{\odot}$  (in blue) to  $50M_{\odot}$  (in yellow).

At present there is no clear consensus on the magnitude of BH kicks. The inferences drawn from the orbital parameters, space velocities, and locations of individual binaries within the Galaxy are inconclusive. While some binary systems, such as Cygnus X-1 and GRS 1915+105, do not require natal BH kicks or suggest only a small kick (Nelemans et al. 1999; Wong et al. 2010; Banagiri et al. 2022), others, like MAXI J1305-704 and XTE J1118+480, indicate large kicks (Brandt et al. 1995; Remillard et al. 2000; Mirabel et al. 2001; Willems et al. 2005a; Gualandris et al. 2005; Fragos et al. 2009; Kimball et al. 2022). Population synthesis studies (Mapelli & Giacobbo 2018; Giacobbo & Mapelli 2018; Chruslinska 2018; Baibhav et al. 2019) indicate that very low kicks are needed for merging compact objects to explain the observed merger rate density from LIGO-Virgo data. Janka (2013) also argued that if kicks are driven by neutrinos they will be suppressed for massive BHs, however, if kicks are driven by explosion asymmetries they can compete with the high kicks experienced by NSs, reaching several hundred

kilometers per second. To accommodate the two extreme scenarios, we explore two extreme kick prescriptions:

**High Kicks:** All BHs, regardless of their other properties, are given a kick randomly drawn from a Maxwellian distribution with an RMS value of  $v_k = 250$  km/s.

**Reduced Kicks:** In this model, we assume that while lighter BHs can receive large kicks, heavier BHs will receive lower kicks to account for the effects of fallback on the formation of BHs. We assume that the more massive the BH, the larger the amount of fallback it experiences, which in turn reduces its natal kick. In this model, we impose that the magnitude of the natal kick decreases linearly from 265 km/s for a  $1.4 M_{\odot}$  NS to 0 km/s for a  $20 M_{\odot}$  BH. In addition, we assume that BHs with masses greater than  $20M_{\odot}$  form via direct collapse of a massive star, and do not receive any natal kicks or mass loss during CC.

### 3.1.3. Spin magnitudes

In section 2, we establish models that describe the direction of the spin. However, determining the magnitude of the spin is significantly more challenging. This is because the mechanisms that influence the magnitude of the spin are not yet well understood. In this article, we will use two models for the spin magnitude.

**Spins triggered by natal kicks:** We have assumed for our two models that the spins of BHs are influenced by some unknown phenomenon related to natal kicks. It is reasonable to assume that the spin magnitude would be directly proportional to the magnitude of the natal kick. Therefore, we have posited that the spin can be expressed as

$$\chi = \hat{\chi} v_{\text{kick}}, \quad (20)$$

where  $\hat{\chi}$  is a constant of proportionality. This relationship is supported by CC simulations by Müller et al. (2019), which have shown a correlation between the magnitude of the kick and the spin magnitude (as depicted in their Fig. 12). This correlation also holds for spin-up caused by off-center explosions proposed by Spruit & Phinney (1998). In this study, we have set the free parameter  $\hat{\chi} = 0.2/100$  for illustrative purposes, indicating that a kick with a magnitude of 100km/s would produce a BH with spin magnitude of 0.2. We will employ this prescription for models **Par** and **Perp**.

**Maxwellian spins:** In addition to kicks, BHs can also be spun through various stochastic processes that increase the spin via a random walk, potentially leading to isotropic spins. In such cases, it is reasonable to expect that the spins would follow a Maxwellian distribution. An example of this is the spinning of stellar cores due to internal gravity waves originating from the convective layer, as suggested by Fuller et al. (2014, 2015); Ma

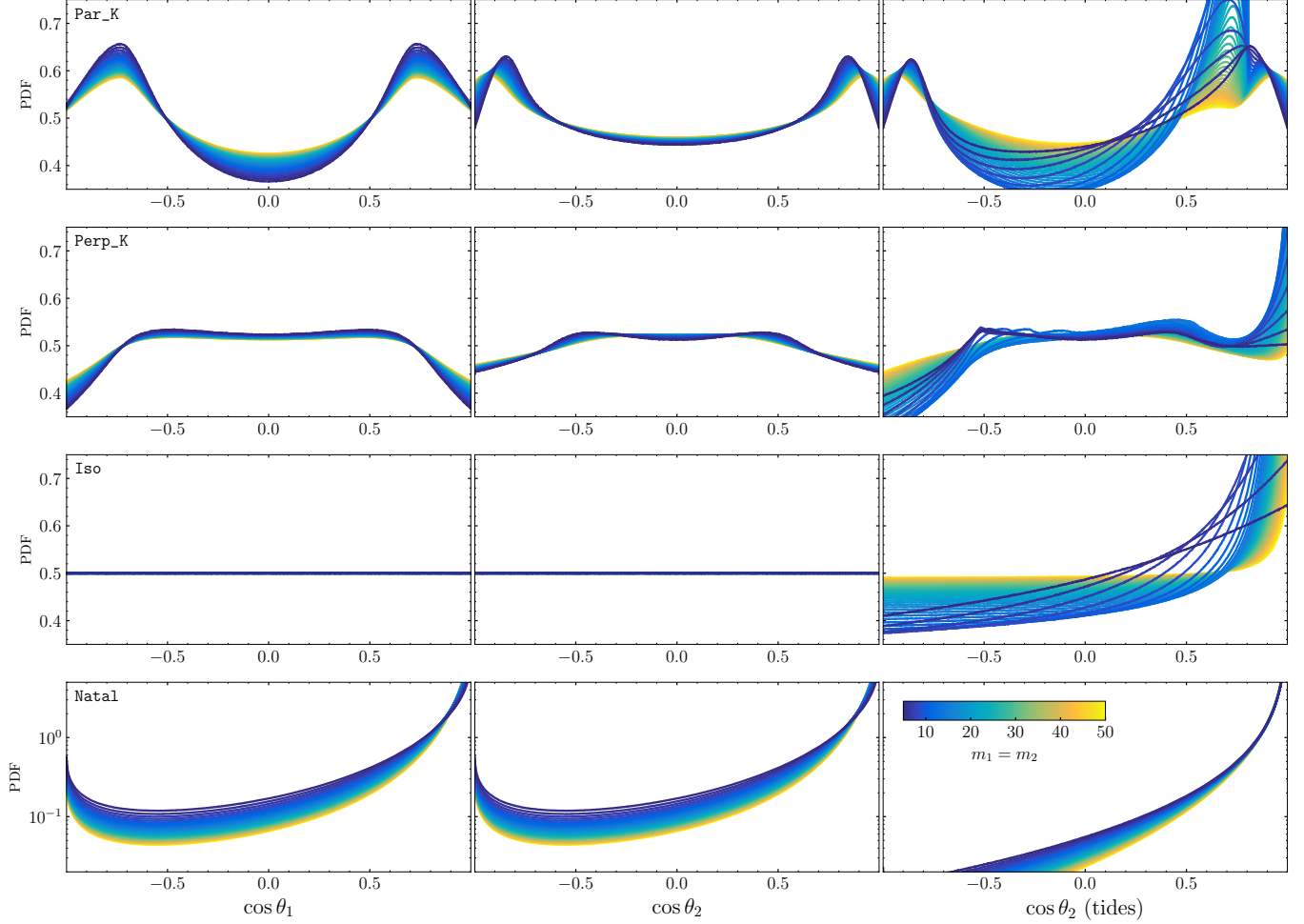


**Figure 7.** PDFs of spin-orbit tilts based on the interacting model for pre-CC2 orbital separations and high kicks for all BH masses:  $p(\cos \theta_1)$  (left),  $p(\cos \theta_2)$  assuming inefficient tides (middle), and  $p(\cos \theta_2)$  with tidal spin up (right) for the **Par**, **Perp**, **Iso**, and **Natal** models (from top to bottom) for BH masses ranging from  $m_1 = m_2 = 5M_\odot$  (in blue) to  $50M_\odot$  (in yellow).

& Fuller (2019); McNeill & Müller (2020). In order to model the **Iso** scenario, we will use a Maxwellian distribution with a root-mean-square mean of 0.2 for the spin magnitudes. We will also use the same distribution for the **Natal** model for simplicity.

#### 3.1.4. Spin tilt evolution and tidal alignment

After CC1, the binary system undergoes changes in its orientation and the BH spin. The post-CC1 spin-orbit misalignment  $\theta_{LS1}$  will depend on the spin models discussed in Sec. 2. The subsequent CC, CC2, will tilt the orbit by  $\cos \theta_{LLi2}$ , and impart spin to the second-born BH for models **Par**, **Perp**, and **Iso**. The tilt of first-born BH with respect to the final orbital angular momentum will change again as

$$\cos \theta_1 = \cos \theta_{LS1} \cos \theta_{LLi2} + \sin \theta_{LS1} \sin \theta_{LLi2} \sin \phi_{S1} \quad (21)$$

where  $\cos \theta_{LS1}$  is spin-orbit misalignment post-CC1, while  $\phi_{S1}$  is sampled uniformly between  $[0, 2\pi]$ . In ad-

dition to previously discussed spin mechanisms, tidal interactions can also contribute to the spin of the BH. Tides can synchronize stellar spins with the binary orbit, potentially resulting in BH spin parallel to the orbital angular momentum after the CC (Hurley et al. 2002). While a detailed treatment of tidal theory in massive stars is beyond the scope of this paper, we consider two possibilities: efficient tidal spin-up of the secondary star along the orbital angular momentum, or completely inefficient tides (Eggleton & Kiseleva-Eggleton 2001; Eggleton 2006).

**No tides:** Since there are no tidal effects, the tilt for second-born BH can be directly calculated as specified in Sec. 2.

**Tides:** In this scenario, we will focus on the tidal effects on the secondary star between the two CC events in the binary evolution. During this phase, if tidal interactions are efficient, they tend to spin the star (but not the BH) with the orbital angular momentum. To model this effect,

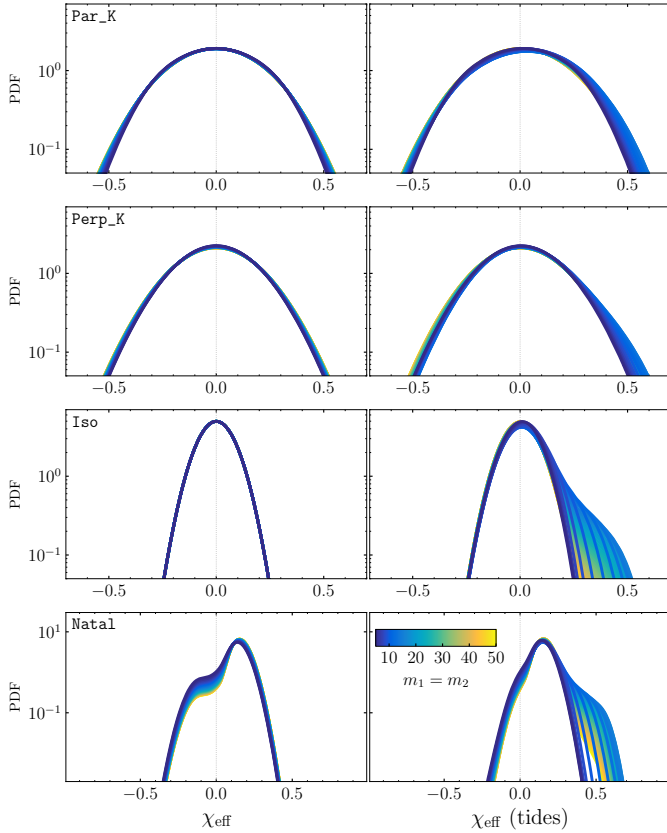


**Figure 8.** PDFs of  $\chi_{\text{eff}}$  based on the interacting model for pre-CC2 orbital separations and high kicks for all BH masses:  $p(\chi_{\text{eff}})$  assuming inefficient tides (left), and  $p(\chi_{\text{eff}})$  with tidal spin up (right) for the **Par**, **Perp**, **Iso**, and **Natal** models (from top to bottom) for BH masses ranging from  $m_1 = m_2 = 5M_\odot$  (in blue) to  $50M_\odot$  (in yellow).

we will use fits of the dimensionless spin of the second-born black hole by [Bavera et al. \(2021\)](#) as a function of binary orbital period, obtained by fitting detailed MESA simulations that accurately tracked the evolution and spin-up of close black hole-Wolf-Rayet systems. The second-born black hole will have two sources of spin: spin along the pre-CC2 orbital angular momentum  $\chi_t$  calculated using fits by [Bavera et al. \(2021\)](#); and spin  $\chi_{2,0}$  due to different processes discussed in Section 2, with a total spin of  $\chi_2 = \chi_t + \chi_{2,0}$ , and spherical angles given by  $(\theta_{LS_2}, \phi_{LS_2})$  with respect to pre-CC2 orbital angular momentum. The misalignment with respect to the final orbital angular momentum is given by

$$\cos \theta_2 = \cos \theta_{LS_2} \cos \theta_{LLi_2} + \sin \theta_{LS_2} \sin \theta_{LLi_2} \sin \phi_{LS_2}, \quad (22)$$

where  $\theta_{LLi_2}$  is the tilt angle between the final and pre-CC2 orbital angular momenta.

### 3.2. Distribution of GW observables

In the previous section, we established a synthetic population, and the next step is to examine how the distribution of various gravitational wave (GW) spin observables changes in response to the processes that drive BHs to spin. Specifically, we will investigate how different prescriptions for factors such as orbital separation, tides, spin magnitudes, and natal kicks will impact spin magnitudes, spin-orbit tilts, and effective inspiral spin.

$$\chi_{\text{eff}} = \frac{m_1 \chi_1 \cos \theta_1 + m_2 \chi_2 \cos \theta_2}{m_1 + m_2} \quad (23)$$

#### 3.2.1. High Kicks

Let us consider the extreme case that BHs receive a natal kick drawn from a Maxwellian distribution with an RMS value of  $v_k = 250 \text{ km/s}$ .

**Non-Interacting binaries:** In this scenario, the binary separation remains unchanged before CC2 and after CC1. We present the spin-orbit tilt distribution in Fig 5, covering a range of BH masses from  $m_1 = m_2 = 5M_\odot$  (shown in blue) to  $50M_\odot$  (shown in yellow). The four panels from top to bottom correspond to models **Par**, **Perp**, **Iso** and **Natal**. The first and second columns display distribution of  $\cos \theta_1$  and  $\cos \theta_2$  assuming inefficient tides, while the third column shows the distribution of  $\cos \theta_2$  if tides are allowed. We find a slight preference for aligned and anti-aligned configurations in  $\cos \theta_{1,2}$  for the **Par** model, whereas the **Perp** model prefers in-plane kicks. This is because in-plane kicks are disfavored, and therefore, if the spins are perpendicular (parallel) to the kicks, they will disfavor spins along (perpendicular to) the orbital angular momentum. The **Iso** mode shows a uniform distribution of  $\cos \theta_{1,2}$ , while the **Natal** model displays mostly aligned BHs with tails extending to larger misalignments. It is worth noting that lighter BHs tend to have larger misalignments in the **Natal** model and greater deviations from isotropy in the **Par** and **Perp** models.

This behavior can be understood as follows: the misalignments in the **Natal** model and deviations from isotropy in the **Par** and **Perp** models depend on  $v_k/v_0 \propto M_i^{-1/2}$ , where  $M_i$  is the total binary mass pre-CC. For binaries that receive the same kick and have the same orbital separation, binaries with a larger total binary mass pre-CC have smaller  $u_k$  and hence smaller misalignments and fewer binary disruptions. Additionally, in the third column of Fig. 5, we also plot the distributions of  $\cos \theta_2$  if tides are allowed, and some binaries get a larger spin component along the orbital angular momentum. This spin up is larger for massive binaries, and in all the 4 models discussed, they tend to be more aligned when tides are allowed.

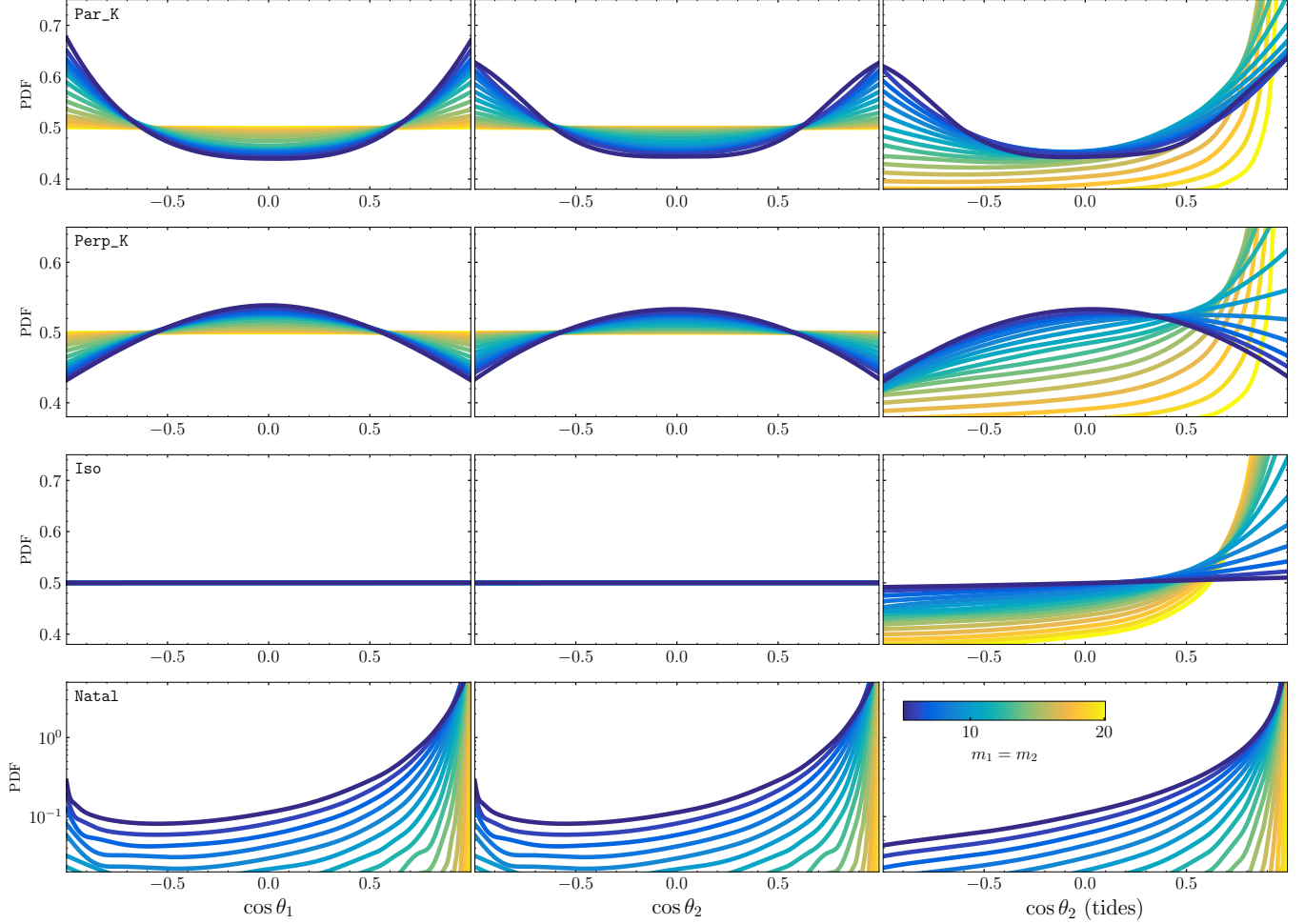


**Figure 9.** PDFs of spin-orbit tilts based on the non-interacting model for pre-CC2 orbital separations and reduced kicks for higher BH masses:  $p(\cos \theta_1)$  (left),  $p(\cos \theta_2)$  assuming inefficient tides (middle), and  $p(\cos \theta_2)$  with tidal spin up (right) for the **Par**, **Perp**, **Iso**, and **Natal** models (from top to bottom) for BH masses ranging from  $m_1 = m_2 = 5M_\odot$  (in blue) to  $20M_\odot$  (in yellow).

In this scenario, all BHs have the same kick distribution, resulting in the same spin magnitude distribution for the **Par** and **Perp** models, regardless of their masses. On the other hand, the spin magnitudes for the **Iso** and **Natal** models follow a Maxwellian distribution. The distribution of  $\chi_{\text{eff}}$  is presented in Fig. 6. For **Iso**, **Perp**, and **Par** models, the distribution of  $\chi_{\text{eff}}$  is symmetric around  $\chi_{\text{eff}} = 0$ , while for **Natal**, it is mostly positive with a tail towards negative values (Gerosa et al. 2018; Callister et al. 2021; Banerjee et al. 2023). Since the spin magnitude distribution for both **Par** and **Perp** models is the same, this results in similar  $\chi_{\text{eff}}$  distributions as well. Moreover, when tides are allowed to spin up the binary, we observe a larger effect in higher mass BH binaries, where their spins tend to be more aligned with the orbital angular momentum and have a positive  $\chi_{\text{eff}}$  distribution.

**Interacting binaries:** Our next assumption is that during the time interval between CC1 and CC2, the binary separation undergoes a change from  $a_{f1}$  to  $a_{i2}$  in such a manner that the separation is reduced enough to enable the BHs to merge within the Hubble time assuming zero eccentricity, once the separation changes again to  $a_{f2}$  after CC2. In Fig. 7 and Fig. 8, we illustrate the spin-orbit tilt distribution and  $\chi_{\text{eff}}$  distributions for a range of BH masses from  $m_1 = m_2 = 5M_\odot$  (shown in blue) to  $50M_\odot$  (shown in yellow). In Fig. 7, we show the four panels from top to bottom corresponding to models **Par**, **Perp**, **Iso** and **Natal**. The first and second columns of each panel display  $\cos \theta_1$  and  $\cos \theta_2$ , assuming inefficient tides, while the third column shows the distribution of  $\cos \theta_2$  if tides are allowed. We find that the spin-orbit misalignment angle, **Par**, has peak tilts from aligned/anti-aligned by around  $40^\circ$  degrees for the first-born BH and  $20^\circ - 30^\circ$  for the second-born BH. On the other hand, the distri-

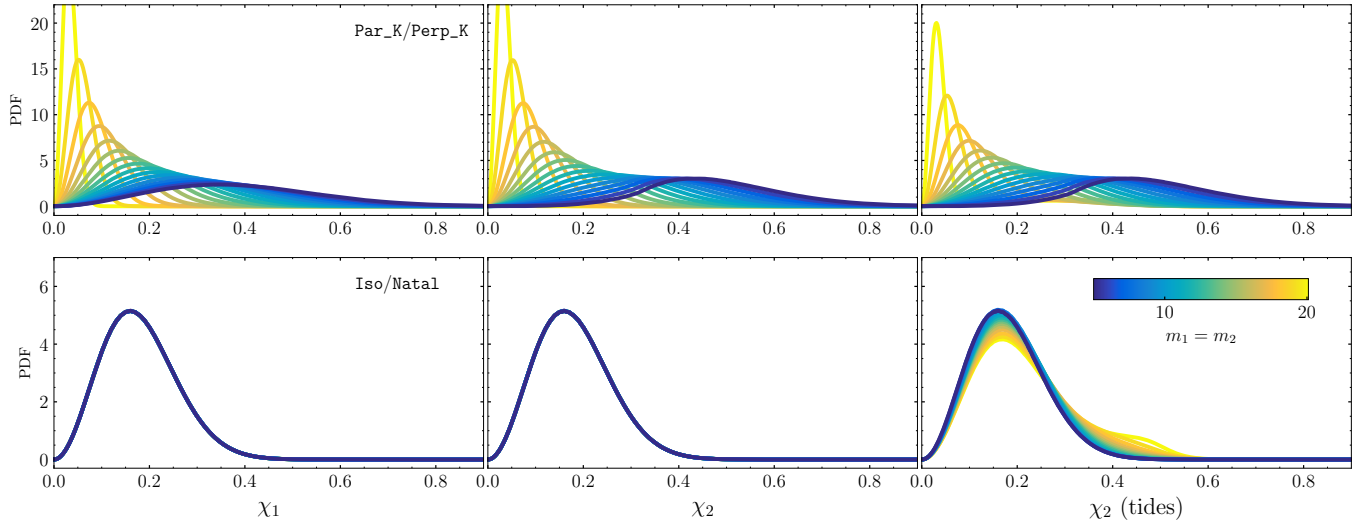


**Figure 10.** PDFs of spin magnitudes based on the non-interacting model for pre-CC2 orbital separations and reduced kicks for higher BH masses:  $p(\chi_1)$  (left),  $p(\chi_2)$  assuming inefficient tides (middle), and  $p(\chi_2)$  with tidal spin up (right) for BH masses ranging from  $m_1 = m_2 = 5M_\odot$  (in blue) to  $20M_\odot$  (in yellow). Top panel shows the distribution for **Par** and **Perp** where spin magnitudes were assumed to be proportional to the natal kick, while the bottom panel shows the distributions for **Iso** and **Natal** models where spin magnitudes are drawn from a Maxwellian distribution.

bution of  $\cos\theta_2$  has less pronounced features because CC2 goes off at much smaller orbital separations. The perpendicular-to-kick spin model, **Perp**, does not prefer aligned or anti-aligned configurations. Once again, tides break the symmetry around  $\cos\theta_2 = 0$ . The distributions we observe are markedly distinct from those in the non-interacting case we presented earlier. This is because the effect of natal kicks is more prominent when the binary’s initial separation is large (assuming the binary remains bound after the CC). In the previous case, if the binary’s initial separation was large, the probability of its orbit shrinking enough to merge within the Hubble time was low. Therefore, binaries with large initial separations were excluded from the distributions of merging binaries. However, in this case, all binaries that survive the first CC merge. After CC1, the binary system undergoes changes in its orientation and spin, which means that even binaries with very large orbital separations after CC1 are included in the distributions shown in Fig 7 and 8.

### 3.2.2. Reduced Kicks

In contrast to the previous section where all BHs received the same kick, in this section, we consider the effect of fallback during formation on the kick received by BHs. Heavier BHs experience more fallback, which results in lower natal kicks. We assume that natal kicks decrease linearly from 265 km/s for a  $1.4 M_\odot$  neutron star to 0 km/s for a  $20 M_\odot$  BH, while BHs with masses greater than  $20M_\odot$  form via direct collapse and do not receive any natal kicks.

**Non-Interacting binaries:** We present the spin-orbit tilt distribution in Fig. 9, covering a range of BH masses from  $m_1 = m_2 = 5M_\odot$  (shown in blue) to  $20M_\odot$  (shown in yellow), assuming that the binary separation remains unchanged between CC1 and CC2. The four panels from top to bottom correspond to models **Par**, **Perp**, **Iso** and **Natal**, with the first and second columns displaying  $\cos\theta_1$  and  $\cos\theta_2$  assuming inefficient tides, while the third column shows the distribution of  $\cos\theta_2$  if tides are allowed. In Fig. 5, when all BHs received high kicks, the deviation from isotropic spin-orbit tilts was more pronounced in lighter BHs compared to heavier ones. However, this effect gets amplified if we assume that lighter BHs receive more kicks compared to heavier ones. This can be observed in Fig. 9, where heavy BHs always appear to be isotropic while lighter ones have a slight preference for aligned/antialigned spins for **Par** and in-plane spins for **Perp**. Additionally, lighter  $5M_\odot$  BHs have longer distribution tails away from  $\cos\theta_{1,2} = 1$ , while heavier BHs are very strictly aligned in **Natal** model, for the same reason.

Since the spin magnitudes in the **Par** and **Perp** models are proportional to kick magnitude and we assume that BHs of different masses receive different natal kick, BHs of different masses should have different spin magnitude distributions. This can be seen in the top panel of Fig. 10, where we plot the distributions of  $\chi_1$ ,  $\chi_2$ , and  $\chi_2$  with spin up by tides for the **Par** and **Perp** models. We observe that for higher masses, the spin magnitudes are small, while for lighter masses, the spin magnitudes are large. This also translates to a correlation between  $\chi_{\text{eff}}$  and

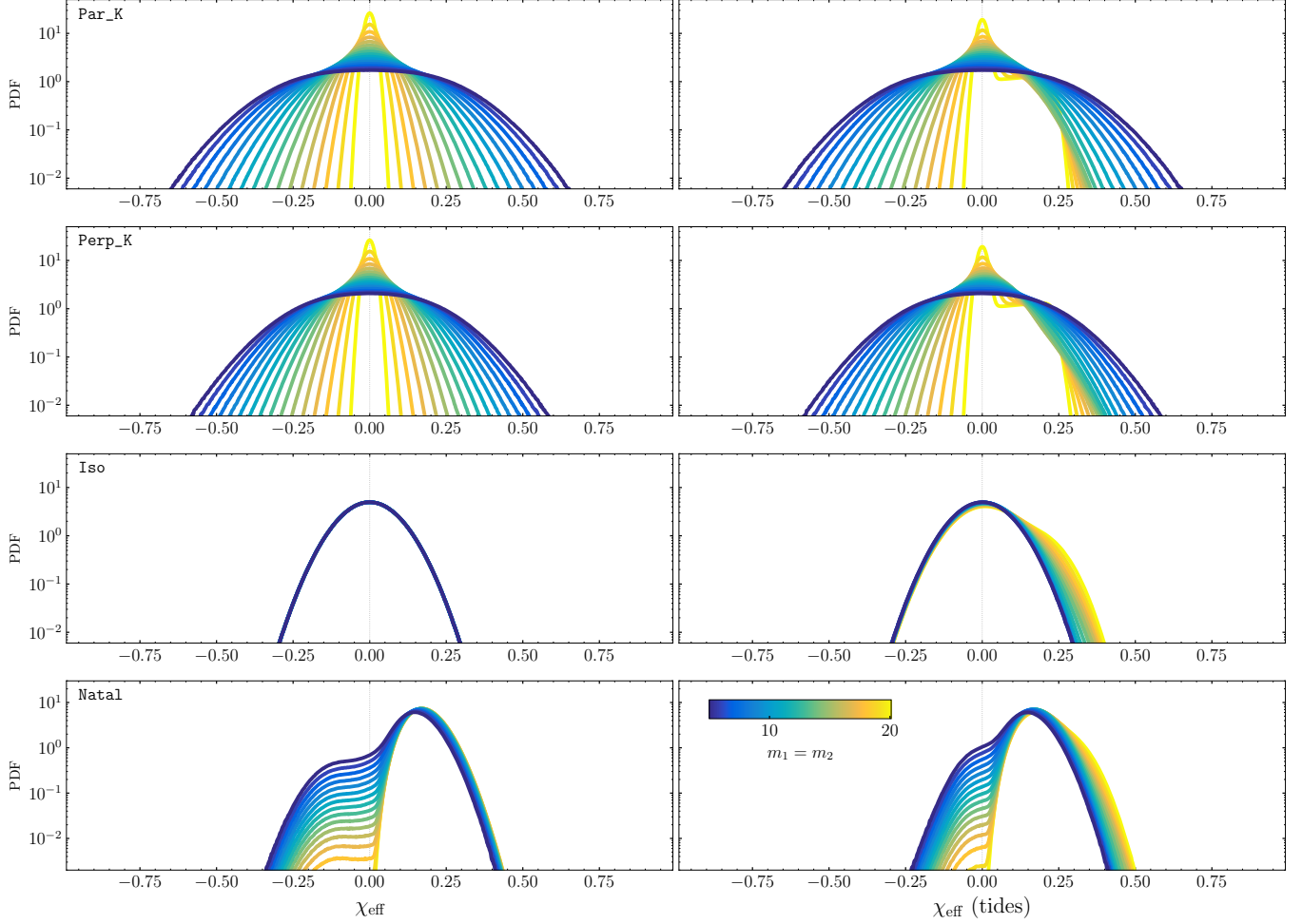


**Figure 11.** PDFs of  $\chi_{\text{eff}}$  based on the non-interacting model for pre-CC2 orbital separations and reduced kicks for higher BH masses:  $p(\chi_{\text{eff}})$  assuming inefficient tides (left), and  $p(\chi_{\text{eff}})$  with tidal spin up (right) for the Par, Perp, Iso, and Natal models (from top to bottom) for BH masses ranging from  $m_1 = m_2 = 5M_{\odot}$  (in blue) to  $50M_{\odot}$  (in yellow).

mass, as shown in Fig 11 for both Par (top panel) and Perp (second panel). We find that as we increase the component masses, the  $\chi_{\text{eff}}$  distribution becomes wider. On the other hand, the spin magnitudes for the Iso and Natal models follow a Maxwellian distribution, as shown in Fig. 10. We also plot the  $\chi_{\text{eff}}$  distribution for these two models in Fig 11. The  $\chi_{\text{eff}}$  distribution in the Iso model is symmetric about  $\chi_{\text{eff}} = 0$ , while the  $\chi_{\text{eff}}$  distribution in the Natal model is mostly positive with a tail towards negative values. In the Natal model, lighter BHs receive larger kicks and have a larger effect of spin-orbit tilts, resulting in larger negative  $\chi_{\text{eff}}$  tails. Furthermore, when tides are allowed to spin up the binary, we observe a larger effect in higher mass BH binaries, where their spins tend to be more aligned with the orbital angular momentum and more binaries have positive  $\chi_{\text{eff}}$  values. **Interacting binaries:** Our next assumption is that any BBHs that survive the first CC will have a post-CC orbital separation small enough to ensure that they

merge within the Hubble time. Fig 12 illustrates the spin-orbit tilt distributions for a range of BH masses, from  $m_1 = m_2 = 5M_{\odot}$  (shown in blue) to  $50M_{\odot}$  (shown in yellow). Fig. 12 displays four panels from top to bottom corresponding to models Par, Perp, Iso and Natal. The first and second columns of each panel display  $\cos\theta_1$  and  $\cos\theta_2$ , respectively, assuming inefficient tides, while the third column shows the distribution of  $\cos\theta_2$  if tides are allowed. The peaks and features of the distributions are qualitatively similar to those shown in Fig. 5, where all BHs received high kicks. However, in this case, heavier BHs receive smaller kicks, resulting in less pronounced peaks and closer-to-isotropic distributions for Par and Perp. We also observe that the inclusion of tides can impact the distribution's symmetry, with the peak at negative  $\cos\theta_2$  being suppressed and the peak at positive  $\cos\theta_2$  being amplified. For example, the peak for  $10M_{\odot}$  BHs lies at  $\theta_2 = 40^\circ$ , where the bin at this peak contains twice as many binaries as if  $\cos\theta_2$  was uniform. Finally,

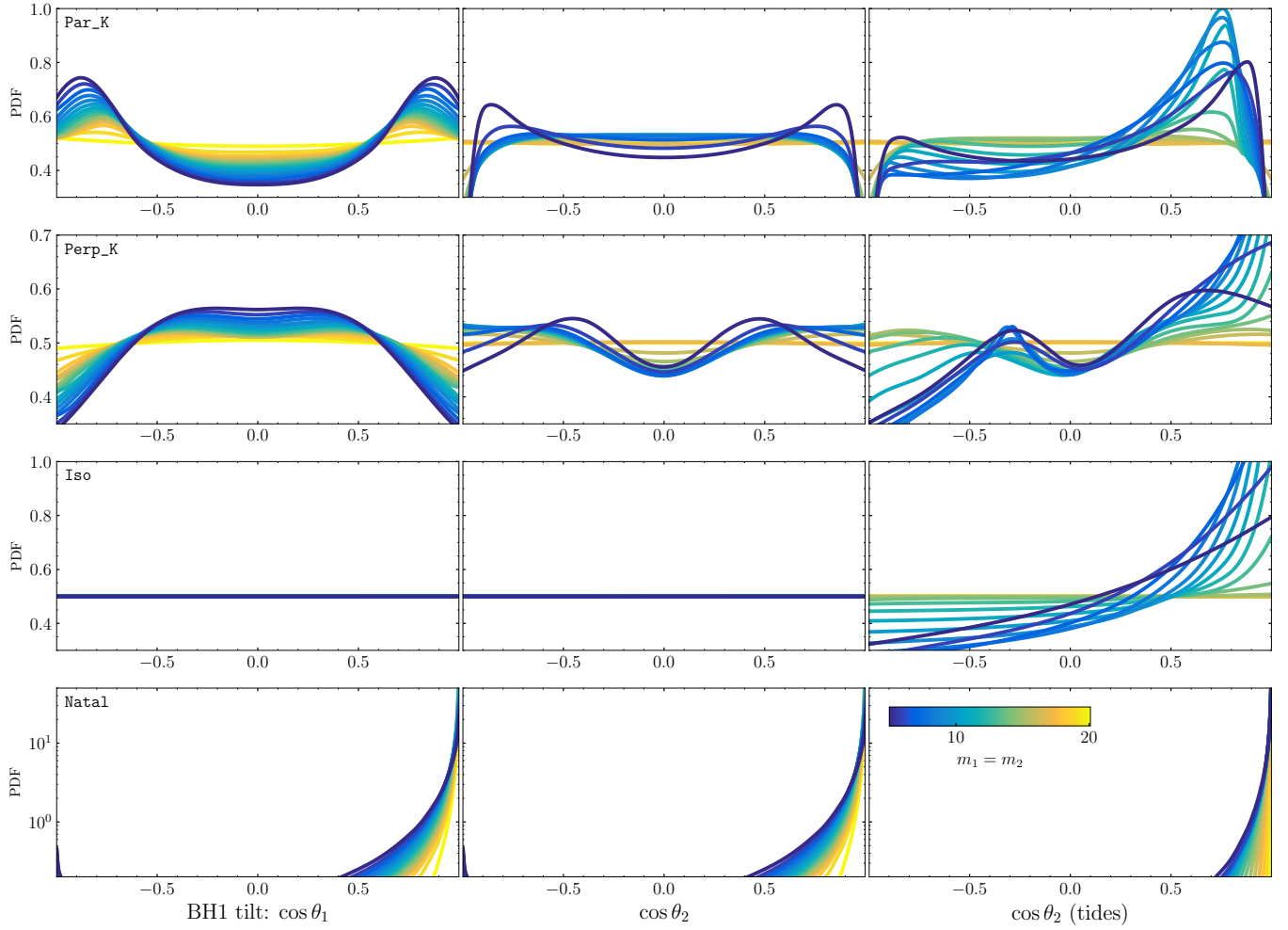


**Figure 12.** PDFs of spin-orbit tilts based on the interacting model for pre-CC2 orbital separations and reduced kicks for higher BH masses:  $p(\cos \theta_1)$  (left),  $p(\cos \theta_2)$  assuming inefficient tides (middle), and  $p(\cos \theta_2)$  with tidal spin up (right) for the **Par**, **Perp**, **Iso**, and **Natal** models (from top to bottom) for BH masses ranging from  $m_1 = m_2 = 5M_\odot$  (in blue) to  $20M_\odot$  (in yellow).

we note that this distribution shares similarities with the spin-orbit tilt distribution of the population observed in GWTC-3, where the spin-orbit tilt distribution peaks at  $60^\circ$  rather than at  $\theta_{1,2} = 0$  (Vitale et al. 2022; Edelman et al. 2023; Callister & Farr 2023). This indicates that BHs may acquire their spins through the same process that generates natal kicks, implying a possible connection between the two phenomena.

#### 4. SUMMARY AND CONCLUSIONS

It’s widely believed that BBHs detected by LVK can be distinguished by their spin orientations: dynamically assembled BBHs typically have isotropic spins, while field binaries often have spins aligned with the orbital angular momentum (Gerosa et al. 2013; Rodriguez et al. 2016; Vitale et al. 2017; Talbot & Thrane 2017; Farr et al. 2017; Stevenson et al. 2017; Farr et al. 2018; Gerosa et al. 2018; Tiwari et al. 2018; Fernandez & Profumo 2019; Baibhav et al. 2022). For field binaries, this is based on the

assumption that the spin of compact objects is inherited from their parent star, which is typically aligned with the orbital angular momentum. In this study, we explore various possibilities that can lead to spin orientations for isolated binaries that are not preferentially aligned with orbital angular momentum. In Section 2, we examine the distribution of spin-orbit tilts for four distinct models pertaining to the origin of BH spins. Each of these models has unique characteristics that depend on the natal kick magnitude.

- **Natal:** BHs inherit their spins from their parent stars. This results in BH spins preferentially aligned with the orbital angular momentum for small kicks, but may have large misalignments for large kicks.
- **Iso:** BH spins have an isotropic distribution.

- **Par**: BH spin and natal kicks are aligned. This leads to slight preference for spins aligned or anti-aligned with orbital angular momentum for small kicks and in-plane spins for large kicks.
- **Perp**: BH spin and natal kicks are perpendicular. This leads to slight preference for in-plane spins for small kicks and aligned or anti-aligned spins for large kicks.

In Section 3, we use our models to make predictions about the distribution of spin-orbit tilts for a synthetic population. We find that the observed distribution is influenced by a complex interplay of various factors such as kick magnitudes, evolutionary history, and tidal interactions. Distinct mechanisms that result in the spin-up of BHs will produce unique signatures in their spin orientations that can be detected in the population of merging BHs observed by LVK. For some of our models, we observe the appearance of two peaks in the spin-orbit tilt distribution. **Iso**, **Perp**, and **Par** have symmetric distributions around  $\cos\theta_{1,2} = 0$ , but this symmetry breaks when we allow tides to spin up the BHs along the orbital angular momentum. This can suppress the peak at  $\cos\theta < 0$  and amplify the peak at  $\cos\theta > 0$ . Interestingly, we find that our models are similar to the LVK observations, which hint at a peak around  $60^\circ$  in the spin-orbit tilt distribution (Vitale et al. 2022; Edelman et al. 2023; Callister & Farr 2023). This supports the notion that BHs may obtain their spins as a result of the kick process. Moreover, these models offer a compelling rationale for the observed distribution of spin-orbit tilts, which is a challenging outcome to explain using alternative formation pathways. The location of the peaks depends on complex combination of mass loss, kick magnitudes, pre-CC orbital separation, and tidal interactions: our assumptions regarding which are oversimplified and may not fully capture the range of complexities encountered in the binary evolution. Thus, a more detailed modeling approach is needed to make comparisons with observations.

In our assumptions, we consider that only one mechanism, in addition to tides, is capable of imparting spins. However, there is a possibility that multiple mechanisms may be at work in different regions of the parameter space. For instance, for low-mass BHs, large kicks could lead to spin-up according to either the **Par** or **Perp** model. On the other hand, for heavy BHs that undergo direct collapse without any asymmetric mass ejection and natal kicks, the infalling convective layers could result in spin-up according to the **Iso** model (as suggested by Gilkis & Soker (2014); Gilkis & Soker (2016); Quataert et al. (2019); Antoni & Quataert (2022, 2023)). This

could result in distinct imprints on spin magnitudes and spin-orbit tilts for varying masses.

If BHs are spun up by kicks during formation, we assume that their spins are proportional to the kicks in one of the models. This leads us to expect a correlation between BH mass and spin magnitudes, i.e. the spin-magnitude increases with the BH mass. Similarly, effective spins have a decreasing width in their distribution with increasing mass. However, this correlation is opposite to that found for primordial BHs, where the effective spin distribution widens with mass (De Luca et al. 2020; Franciolini & Pani 2022). Although no strong correlations have been found between BH mass and effective spin or spin magnitude, future GW observing runs may reveal more obscure features and correlations in even hard-to-measure parameters. It is also possible that only one of our assumptions about spin magnitude and spin-orbit tilt holds. For example, the spin-kick alignment model by Janka et al. (2022) does not have spin proportional to kicks. In that case, despite the characteristic spin-orbit tilt distribution in the **Par** model, one might not find the correlation between mass and individual BH spins or effective spins. On the other hand, Müller et al. (2019) found an isotropic distribution for spin-orbit tilts but spins proportional to kicks. In that case, even the isotropic-spin model will have mass-spin correlations opposite to what was assumed here. While large kicks lead to more conspicuous spin-orbit tilt and spin magnitude distributions, they also tend to disrupt the binaries. Binaries that receive small kicks can survive, but the features in spin distribution are less noticeable. Moreover, the measurement of BH spins is a challenging task, which makes it difficult to study and resolve obscure features related to them.

One key implication of our study is that it challenges the conventional wisdom that isolated binary evolution can only produce BBHs with preferentially aligned spins. According to this widely held notion, GW events with large spin-orbit misalignments, such as GW190412, GW190521, and GW191109, can arise only in dense stellar clusters or galactic centers (Gerosa et al. 2020; Rodriguez et al. 2020; Tagawa et al. 2020; Baibhav et al. 2020; Liu & Lai 2021; Gerosa et al. 2021; Mapelli et al. 2021; Gerosa & Fishbach 2021; Baibhav et al. 2021; Mapelli et al. 2022; Fishbach et al. 2022; Li et al. 2023; Zhang et al. 2023). Our study challenges this notion and argues that these binaries could also originate in the field. The identification of precession or  $\chi_{\text{eff}} < 0$  in isolated binary mergers – traditionally considered highly unlikely – is a distinct possibility. This also suggests that distinguishing between binaries that evolve in isolation

versus those that are dynamically assembled based solely on their spin directions is considerably more challenging.

The orientation of spin in BBHs not only provides insights into their origin but also helps understand the mechanisms that give BHs their spin. The way BHs get their spin affects the distribution of parameters like  $\chi_{1,2}$ ,  $\theta_{1,2}$ , and  $\chi_{\text{eff}}$ . Analyzing these distributions can provide important information about the exact mechanisms behind BH spin generation. With the upcoming observing runs of LIGO and future detectors, we have a unique opportunity to solve the mysteries surrounding BH spins. By studying the imprints left by the process of BH spin generation, we can improve our understanding of the complex processes that govern their formation.

#### ACKNOWLEDGEMENTS

V.B. acknowledges support from CIERA, Northwestern University and the NASA Hubble Fellowship grant HST-HF2-51548.001-A awarded by the Space Telescope Science Institute, which is operated by the Association of Universities for Research in Astronomy, Inc., for NASA, under contract NAS5-26555. V.K. was supported by the Gordon and Betty Moore Foundation (grant awards GBMF8477 and GBMF12341), through a Guggenheim Fellowship, and the D.I. Linzer Distinguished University Professorship fund. This research was supported in part through the computational resources and staff contributions provided for the Quest high performance computing facility at Northwestern University which is jointly supported by the Office of the Provost, the Office for Research, and Northwestern University Information Technology.

#### REFERENCES

- Albrecht, S., Reffert, S., Snellen, I., Quirrenbach, A., & Mitchell, D. S. 2007, *Astron. Astrophys.*, 474, 565, doi: [10.1051/0004-6361:20077953](https://doi.org/10.1051/0004-6361:20077953)
- Albrecht, S., Reffert, S., Snellen, I. A. G., & Winn, J. N. 2009, *Nature*, 461, 373, doi: [10.1038/nature08408](https://doi.org/10.1038/nature08408)
- Albrecht, S., Setiawan, J., Torres, G., Fabrycky, D. C., & Winn, J. N. 2013, *Astrophys. J.*, 767, 32, doi: [10.1088/0004-637X/767/1/32](https://doi.org/10.1088/0004-637X/767/1/32)
- Albrecht, S., Winn, J., Carter, J., Snellen, I., & de Mooij, E. 2011, *Astrophys. J.*, 726, 68, doi: [10.1088/0004-637X/726/2/68](https://doi.org/10.1088/0004-637X/726/2/68)
- Albrecht, S., et al. 2014, *Astrophys. J.*, 785, 83, doi: [10.1088/0004-637X/785/2/83](https://doi.org/10.1088/0004-637X/785/2/83)
- Antoni, A., & Quataert, E. 2022, *Mon. Not. Roy. Astron. Soc.*, 511, 176, doi: [10.1093/mnras/stab3776](https://doi.org/10.1093/mnras/stab3776)
- . 2023. <https://arxiv.org/abs/2301.05237>
- Arzoumanian, Z., Chernoffs, D. F., & Cordes, J. M. 2002, *Astrophys. J.*, 568, 289, doi: [10.1086/338805](https://doi.org/10.1086/338805)
- Atri, P., et al. 2019, *Mon. Not. Roy. Astron. Soc.*, 489, 3116, doi: [10.1093/mnras/stz2335](https://doi.org/10.1093/mnras/stz2335)
- Baibhav, V., Berti, E., Gerosa, D., et al. 2019, *Phys. Rev. D*, 100, 064060, doi: [10.1103/PhysRevD.100.064060](https://doi.org/10.1103/PhysRevD.100.064060)
- Baibhav, V., Berti, E., Gerosa, D., Mould, M., & Wong, K. W. K. 2021, *Phys. Rev. D*, 104, 084002, doi: [10.1103/PhysRevD.104.084002](https://doi.org/10.1103/PhysRevD.104.084002)
- Baibhav, V., Doctor, Z., & Kalogera, V. 2022. <https://arxiv.org/abs/2212.12113>
- Baibhav, V., Gerosa, D., Berti, E., et al. 2020, *Phys. Rev. D*, 102, 043002, doi: [10.1103/PhysRevD.102.043002](https://doi.org/10.1103/PhysRevD.102.043002)
- Banagiri, S., Doctor, Z., Kalogera, V., Kimball, C., & Andrews, J. J. 2022. <https://arxiv.org/abs/2211.16361>
- Banerjee, S., Olejak, A., & Belczynski, K. 2023. <https://arxiv.org/abs/2302.10851>
- Bavera, S. S., Zevin, M., & Fragos, T. 2021. <https://arxiv.org/abs/2105.09077>
- Bisnovatyi-Kogan, G. S. 1993, *Astron. Astrophys. Trans.*, 3, 287, doi: [10.1080/10556799308230566](https://doi.org/10.1080/10556799308230566)
- Blondin, J. M., & Mezzacappa, A. 2007, *Nature*, 445, 58, doi: [10.1038/nature05428](https://doi.org/10.1038/nature05428)
- Brandt, N., & Podsiadlowski, P. 1995, *MNRAS*, 274, 461, doi: [10.1093/mnras/274.2.461](https://doi.org/10.1093/mnras/274.2.461)
- Brandt, W. N., Podsiadlowski, P., & Sigurdsson, S. 1995, *MNRAS*, 277, L35, doi: [10.1093/mnras/277.1.L35](https://doi.org/10.1093/mnras/277.1.L35)
- Breton, R. P., Kaspi, V. M., Kramer, M., et al. 2008, *Science*, 321, 104, doi: [10.1126/science.1159295](https://doi.org/10.1126/science.1159295)
- Burrows, A., & Hayes, J. 1996, *Phys. Rev. Lett.*, 76, 352, doi: [10.1103/PhysRevLett.76.352](https://doi.org/10.1103/PhysRevLett.76.352)
- Burrows, A., Vartanyan, D., & Wang, T. 2023, *Astrophys. J.*, 957, 68, doi: [10.3847/1538-4357/acfc1c](https://doi.org/10.3847/1538-4357/acfc1c)
- Burrows, A., Wang, T., Vartanyan, D., & Coleman, M. S. B. 2024, *Astrophys. J.*, 963, 63, doi: [10.3847/1538-4357/ad2353](https://doi.org/10.3847/1538-4357/ad2353)
- Callister, T. A., & Farr, W. M. 2023. <https://arxiv.org/abs/2302.07289>
- Callister, T. A., Farr, W. M., & Renzo, M. 2021, *Astrophys. J.*, 920, 157, doi: [10.3847/1538-4357/ac1347](https://doi.org/10.3847/1538-4357/ac1347)
- Cantiello, M., Mankovich, C., Bildsten, L., Christensen-Dalsgaard, J., & Paxton, B. 2014, *ApJ*, 788, 93, doi: [10.1088/0004-637X/788/1/93](https://doi.org/10.1088/0004-637X/788/1/93)
- Chan, C., Müller, B., & Heger, A. 2020, *Mon. Not. Roy. Astron. Soc.*, 495, 3751, doi: [10.1093/mnras/staa1431](https://doi.org/10.1093/mnras/staa1431)
- Chatterjee, S., Vlemmings, W. H. T., Briskin, W. F., et al. 2005, *Astrophys. J. Lett.*, 630, L61, doi: [10.1086/491701](https://doi.org/10.1086/491701)

- Chatterjee, S., Briskin, W. F., Vlemmings, W. H. T., et al. 2009, *Astrophys. J.*, 698, 250, doi: [10.1088/0004-637X/698/1/250](https://doi.org/10.1088/0004-637X/698/1/250)
- Chruslinska, M. 2018, *IAU Symp.*, 433, doi: [10.1017/S1743921318007639](https://doi.org/10.1017/S1743921318007639)
- Coleman, M. S. B., & Burrows, A. 2022, *Mon. Not. Roy. Astron. Soc.*, 517, 3938, doi: [10.1093/mnras/stac2573](https://doi.org/10.1093/mnras/stac2573)
- De Luca, V., Franciolini, G., Pani, P., & Riotto, A. 2020, *JCAP*, 04, 052, doi: [10.1088/1475-7516/2020/04/052](https://doi.org/10.1088/1475-7516/2020/04/052)
- Desvignes, G., Kramer, M., Lee, K., et al. 2019, *Science*, 365, 1013, doi: [10.1126/science.aav7272](https://doi.org/10.1126/science.aav7272)
- Edelman, B., Farr, B., & Doctor, Z. 2023, *Astrophys. J.*, 946, 16, doi: [10.3847/1538-4357/acb5ed](https://doi.org/10.3847/1538-4357/acb5ed)
- Eggenberger, P., Buldgen, G., & Salmon, S. J. A. J. 2019, *A&A*, 626, L1, doi: [10.1051/0004-6361/201935509](https://doi.org/10.1051/0004-6361/201935509)
- Eggleton, P. 2006, *Evolutionary Processes in Binary and Multiple Stars*
- Eggleton, P. P., & Kiseleva-Eggleton, L. 2001, *ApJ*, 562, 1012, doi: [10.1086/323843](https://doi.org/10.1086/323843)
- Farr, B., Holz, D. E., & Farr, W. M. 2018, *Astrophys. J. Lett.*, 854, L9, doi: [10.3847/2041-8213/aaaa64](https://doi.org/10.3847/2041-8213/aaaa64)
- Farr, W. M., Kremer, K., Lyutikov, M., & Kalogera, V. 2011, *ApJ*, 742, 81, doi: [10.1088/0004-637X/742/2/81](https://doi.org/10.1088/0004-637X/742/2/81)
- Farr, W. M., Stevenson, S., Coleman Miller, M., et al. 2017, *Nature*, 548, 426, doi: [10.1038/nature23453](https://doi.org/10.1038/nature23453)
- Faucher-Giguere, C.-A., & Kaspi, V. M. 2006, *Astrophys. J.*, 643, 332, doi: [10.1086/501516](https://doi.org/10.1086/501516)
- Fernandez, N., & Profumo, S. 2019, *JCAP*, 08, 022, doi: [10.1088/1475-7516/2019/08/022](https://doi.org/10.1088/1475-7516/2019/08/022)
- Fernandez, R. 2010, *Astrophys. J.*, 725, 1563, doi: [10.1088/0004-637X/725/2/1563](https://doi.org/10.1088/0004-637X/725/2/1563)
- Fishbach, M., Kimball, C., & Kalogera, V. 2022, *Astrophys. J. Lett.*, 935, L26, doi: [10.3847/2041-8213/ac86c4](https://doi.org/10.3847/2041-8213/ac86c4)
- Fragione, G., & Loeb, A. 2023, *Astrophys. J.*, 958, 130, doi: [10.3847/1538-4357/ad083b](https://doi.org/10.3847/1538-4357/ad083b)
- Fragos, T., Tremmel, M., Rantsiou, E., & Belczynski, K. 2010, *Astrophys. J. Lett.*, 719, L79, doi: [10.1088/2041-8205/719/1/L79](https://doi.org/10.1088/2041-8205/719/1/L79)
- Fragos, T., Willems, B., Kalogera, V., et al. 2009, *Astrophys. J.*, 697, 1057, doi: [10.1088/0004-637X/697/2/1057](https://doi.org/10.1088/0004-637X/697/2/1057)
- Franciolini, G., & Pani, P. 2022, *Phys. Rev. D*, 105, 123024, doi: [10.1103/PhysRevD.105.123024](https://doi.org/10.1103/PhysRevD.105.123024)
- Fryer, C., Burrows, A., & Benz, W. 1998, *Astrophys. J.*, 496, 333, doi: [10.1086/305348](https://doi.org/10.1086/305348)
- Fryer, C. L., & Kusenko, A. 2006, *Astrophys. J. Suppl.*, 163, 335, doi: [10.1086/500933](https://doi.org/10.1086/500933)
- Fuller, J., Cantiello, M., Lecoanet, D., & Quataert, E. 2015, *ApJ*, 810, 101, doi: [10.1088/0004-637X/810/2/101](https://doi.org/10.1088/0004-637X/810/2/101)
- Fuller, J., Lecoanet, D., Cantiello, M., & Brown, B. 2014, *ApJ*, 796, 17, doi: [10.1088/0004-637X/796/1/17](https://doi.org/10.1088/0004-637X/796/1/17)
- Fuller, J., & Ma, L. 2019, *Astrophys. J. Lett.*, 881, L1, doi: [10.3847/2041-8213/ab339b](https://doi.org/10.3847/2041-8213/ab339b)
- Gerosa, D., Berti, E., O’Shaughnessy, R., et al. 2018, *Phys. Rev. D*, 98, 084036, doi: [10.1103/PhysRevD.98.084036](https://doi.org/10.1103/PhysRevD.98.084036)
- Gerosa, D., & Fishbach, M. 2021, *Nature Astron.*, 5, 749, doi: [10.1038/s41550-021-01398-w](https://doi.org/10.1038/s41550-021-01398-w)
- Gerosa, D., Giacobbo, N., & Vecchio, A. 2021, *Astrophys. J.*, 915, 56, doi: [10.3847/1538-4357/ac00bb](https://doi.org/10.3847/1538-4357/ac00bb)
- Gerosa, D., Kesden, M., Berti, E., O’Shaughnessy, R., & Sperhake, U. 2013, *Phys. Rev. D*, 87, 104028, doi: [10.1103/PhysRevD.87.104028](https://doi.org/10.1103/PhysRevD.87.104028)
- Gerosa, D., Vitale, S., & Berti, E. 2020, *Phys. Rev. Lett.*, 125, 101103, doi: [10.1103/PhysRevLett.125.101103](https://doi.org/10.1103/PhysRevLett.125.101103)
- Gessner, A., & Janka, H.-T. 2018, *Astrophys. J.*, 865, 61, doi: [10.3847/1538-4357/aadb4e](https://doi.org/10.3847/1538-4357/aadb4e)
- Giacobbo, N., & Mapelli, M. 2018, *Mon. Not. Roy. Astron. Soc.*, 480, 2011, doi: [10.1093/mnras/sty1999](https://doi.org/10.1093/mnras/sty1999)
- Gilkis, A., & Soker, N. 2014, *Mon. Not. Roy. Astron. Soc.*, 439, 4011, doi: [10.1093/mnras/stu257](https://doi.org/10.1093/mnras/stu257)
- Gilkis, A., & Soker, N. 2016, *ApJ*, 827, 40, doi: [10.3847/0004-637X/827/1/40](https://doi.org/10.3847/0004-637X/827/1/40)
- Gompertz, B. P., Nicholl, M., Schmidt, P., Pratten, G., & Vecchio, A. 2022, *Mon. Not. Roy. Astron. Soc.*, 511, 1454, doi: [10.1093/mnras/stac029](https://doi.org/10.1093/mnras/stac029)
- Gualandris, A., Colpi, M., Portegies Zwart, S., & Possenti, A. 2005, *Astrophys. J.*, 618, 845, doi: [10.1086/426126](https://doi.org/10.1086/426126)
- Guilet, J., & Fernández, R. 2014, *Mon. Not. Roy. Astron. Soc.*, 441, 2782, doi: [10.1093/mnras/stu718](https://doi.org/10.1093/mnras/stu718)
- Harrison, P. A., Lyne, A. G., & Anderson, B. 1993, *MNRAS*, 261, 113, doi: [10.1093/mnras/261.1.113](https://doi.org/10.1093/mnras/261.1.113)
- Heger, A., Woosley, S. E., & Spruit, H. C. 2005, *Astrophys. J.*, 626, 350, doi: [10.1086/429868](https://doi.org/10.1086/429868)
- Hobbs, G., Lorimer, D. R., Lyne, A. G., & Kramer, M. 2005, *Mon. Not. Roy. Astron. Soc.*, 360, 974, doi: [10.1111/j.1365-2966.2005.09087.x](https://doi.org/10.1111/j.1365-2966.2005.09087.x)
- Hurley, J. R., Tout, C. A., & Pols, O. R. 2002, *MNRAS*, 329, 897, doi: [10.1046/j.1365-8711.2002.05038.x](https://doi.org/10.1046/j.1365-8711.2002.05038.x)
- Igoshev, A. P., Chruslinska, M., Dorozsmai, A., & Toonen, S. 2021, *Mon. Not. Roy. Astron. Soc.*, 508, 3345, doi: [10.1093/mnras/stab2734](https://doi.org/10.1093/mnras/stab2734)
- Janka, H. T. 2013, *Mon. Not. Roy. Astron. Soc.*, 434, 1355, doi: [10.1093/mnras/stt1106](https://doi.org/10.1093/mnras/stt1106)
- . 2017, *Astrophys. J.*, 837, 84, doi: [10.3847/1538-4357/aa618e](https://doi.org/10.3847/1538-4357/aa618e)
- Janka, H. T., & Mueller, E. 1994, *A&A*, 290, 496
- Janka, H.-T., Wongwathanarat, A., & Kramer, M. 2022, *Astrophys. J.*, 926, 9, doi: [10.3847/1538-4357/ac403c](https://doi.org/10.3847/1538-4357/ac403c)
- Johnston, S., Hobbs, G., Vigeland, S., et al. 2005, *Mon. Not. Roy. Astron. Soc.*, 364, 1397, doi: [10.1111/j.1365-2966.2005.09669.x](https://doi.org/10.1111/j.1365-2966.2005.09669.x)

- Johnston, S., Kramer, M., Karastergiou, A., et al. 2007, *Mon. Not. Roy. Astron. Soc.*, 381, 1625, doi: [10.1111/j.1365-2966.2007.12352.x](https://doi.org/10.1111/j.1365-2966.2007.12352.x)
- Kalogera, V. 1996, *Astrophys. J.*, 471, 352, doi: [10.1086/177974](https://doi.org/10.1086/177974)
- . 2000, *Astrophys. J.*, 541, 319, doi: [10.1086/309400](https://doi.org/10.1086/309400)
- Kapil, V., Mandel, I., Berti, E., & Müller, B. 2023, *Mon. Not. Roy. Astron. Soc.*, 519, 5893, doi: [10.1093/mnras/stad019](https://doi.org/10.1093/mnras/stad019)
- Kaspi, V. M., Bailes, M., Manchester, R. N., Stappers, B. W., & Bell, J. F. 1996, *Nature*, 381, 584, doi: [10.1038/381584a0](https://doi.org/10.1038/381584a0)
- Kaspi, V. M., & Helfand, D. J. 2002, *ASP Conf. Ser.*, 271, 3, <https://arxiv.org/abs/astro-ph/0201183>
- Kazeroni, R., Guilet, J., & Foglizzo, T. 2016, *Mon. Not. Roy. Astron. Soc.*, 456, 126, doi: [10.1093/mnras/stv2666](https://doi.org/10.1093/mnras/stv2666)
- . 2017, *Mon. Not. Roy. Astron. Soc.*, 471, 914, doi: [10.1093/mnras/stx1566](https://doi.org/10.1093/mnras/stx1566)
- Kimball, C., et al. 2022. <https://arxiv.org/abs/2211.02158>
- Kramer, M., Lyne, A. G., Hobbs, G., et al. 2003, *Astrophys. J. Lett.*, 593, L31, doi: [10.1086/378082](https://doi.org/10.1086/378082)
- Kusenko, A., Mandal, B. P., & Mukherjee, A. 2008, *Phys. Rev. D*, 77, 123009, doi: [10.1103/PhysRevD.77.123009](https://doi.org/10.1103/PhysRevD.77.123009)
- Lai, D., Chernoff, D. F., & Cordes, J. M. 2001, *Astrophys. J.*, 549, 1111, doi: [10.1086/319455](https://doi.org/10.1086/319455)
- Li, G.-P., Lin, D.-B., & Yuan, Y. 2023, *Phys. Rev. D*, 107, 063007, doi: [10.1103/PhysRevD.107.063007](https://doi.org/10.1103/PhysRevD.107.063007)
- Liu, B., & Lai, D. 2021, *Mon. Not. Roy. Astron. Soc.*, 502, 2049, doi: [10.1093/mnras/stab178](https://doi.org/10.1093/mnras/stab178)
- Lyne, A. G., & Lorimer, D. R. 1994, *Nature*, 369, 127, doi: [10.1038/369127a0](https://doi.org/10.1038/369127a0)
- Ma, L., & Fuller, J. 2019, *Mon. Not. Roy. Astron. Soc.*, 488, 4338, doi: [10.1093/mnras/stz2009](https://doi.org/10.1093/mnras/stz2009)
- Mandel, I., & Igoshev, A. P. 2023, *Astrophys. J.*, 944, 153, doi: [10.3847/1538-4357/acb3c3](https://doi.org/10.3847/1538-4357/acb3c3)
- Mandel, I., & Müller, B. 2020, *Mon. Not. Roy. Astron. Soc.*, 499, 3214, doi: [10.1093/mnras/staa3043](https://doi.org/10.1093/mnras/staa3043)
- Mapelli, M., Bouffanais, Y., Santoliquido, F., Sedda, M. A., & Artale, M. C. 2022, *Mon. Not. Roy. Astron. Soc.*, 511, 5797, doi: [10.1093/mnras/stac422](https://doi.org/10.1093/mnras/stac422)
- Mapelli, M., & Giacobbo, N. 2018, *Mon. Not. Roy. Astron. Soc.*, 479, 4391, doi: [10.1093/mnras/sty1613](https://doi.org/10.1093/mnras/sty1613)
- Mapelli, M., et al. 2021, *Mon. Not. Roy. Astron. Soc.*, 505, 339, doi: [10.1093/mnras/stab1334](https://doi.org/10.1093/mnras/stab1334)
- Marcussen, M. L., & Albrecht, S. H. 2022, *ApJ*, 933, 227, doi: [10.3847/1538-4357/ac75c2](https://doi.org/10.3847/1538-4357/ac75c2)
- Marcussen, M. L., Albrecht, S. H., Winn, J. N., et al. 2024, *ApJ*, 975, 149, doi: [10.3847/1538-4357/ad75fa](https://doi.org/10.3847/1538-4357/ad75fa)
- Marques, J. P., Goupil, M. J., Lebreton, Y., et al. 2013, *A&A*, 549, A74, doi: [10.1051/0004-6361/201220211](https://doi.org/10.1051/0004-6361/201220211)
- Matese, J. J., & Whitmire, D. P. 1983, *ApJ*, 266, 776, doi: [10.1086/160825](https://doi.org/10.1086/160825)
- McNeill, L. O., & Müller, B. 2020, *Mon. Not. Roy. Astron. Soc.*, 497, 4644, doi: [10.1093/mnras/staa2287](https://doi.org/10.1093/mnras/staa2287)
- Mirabel, I. F., Dhawan, V., Mignani, R. P., Rodrigues, I., & Guglielmetti, F. 2001, *Nature*, 413, 139, doi: [10.1038/35093060](https://doi.org/10.1038/35093060)
- Moreno Méndez, E., & Cantiello, M. 2016, *New Astron.*, 44, 58, doi: [10.1016/j.newast.2015.09.007](https://doi.org/10.1016/j.newast.2015.09.007)
- Müller, B. 2023, *Mon. Not. Roy. Astron. Soc.*, 526, 2880, doi: [10.1093/mnras/stad2881](https://doi.org/10.1093/mnras/stad2881)
- Müller, B., Melson, T., Heger, A., & Janka, H. T. 2017, *Mon. Not. Roy. Astron. Soc.*, 472, 491, doi: [10.1093/mnras/stx1962](https://doi.org/10.1093/mnras/stx1962)
- Müller, B., Tauris, T. M., Heger, A., et al. 2019, *Mon. Not. Roy. Astron. Soc.*, 484, 3307, doi: [10.1093/mnras/stz216](https://doi.org/10.1093/mnras/stz216)
- Nelemans, G., Tauris, T. M., & van den Heuvel, E. P. J. 1999, *Astron. Astrophys.*, 352, L87, <https://arxiv.org/abs/astro-ph/9911054>
- Ng, C. Y., & Romani, R. W. 2007, *Astrophys. J.*, 660, 1357, doi: [10.1086/513597](https://doi.org/10.1086/513597)
- Ng, C.-Y., Romani, R. W., Brisken, W. F., Chatterjee, S., & Kramer, M. 2006, *Astrophys. J.*, 654, 487, doi: [10.1086/510576](https://doi.org/10.1086/510576)
- Noutsos, A., Kramer, M., Carr, P., & Johnston, S. 2012, *Mon. Not. Roy. Astron. Soc.*, 423, 2736, doi: [10.1111/j.1365-2966.2012.21083.x](https://doi.org/10.1111/j.1365-2966.2012.21083.x)
- Noutsos, A., Schnitzeler, D. H. F. M., Keane, E. F., Kramer, M., & Johnston, S. 2013, *MNRAS*, 430, 2281, doi: [10.1093/mnras/stt047](https://doi.org/10.1093/mnras/stt047)
- O'Doherty, T. N., Bahramian, A., Miller-Jones, J. C. A., et al. 2023, doi: [10.1093/mnras/stad680](https://doi.org/10.1093/mnras/stad680)
- O'Shaughnessy, R., Gerosa, D., & Wysocki, D. 2017, *Phys. Rev. Lett.*, 119, 011101, doi: [10.1103/PhysRevLett.119.011101](https://doi.org/10.1103/PhysRevLett.119.011101)
- Ott, C. D., Burrows, A., Dessart, L., & Livne, E. 2006, *Phys. Rev. Lett.*, 96, 201102, doi: [10.1103/PhysRevLett.96.201102](https://doi.org/10.1103/PhysRevLett.96.201102)
- Popov, S. B., Boldin, P. A., Miralles, J. A., Pons, J. A., & Posselt, B. 2011, *AIP Conf. Proc.*, 1379, 148, doi: [10.1063/1.3629503](https://doi.org/10.1063/1.3629503)
- Popov, S. B., & Turolla, R. 2012, *ASP Conf. Ser.*, 466, 191, <https://arxiv.org/abs/1206.2819>
- Poutanen, J., et al. 2022, *Science*, 375, ab14679, doi: [10.1126/science.ab14679](https://doi.org/10.1126/science.ab14679)
- Powell, J., & Müller, B. 2020, *Mon. Not. Roy. Astron. Soc.*, 494, 4665, doi: [10.1093/mnras/staa1048](https://doi.org/10.1093/mnras/staa1048)
- Quataert, E., Lecoanet, D., & Coughlin, E. R. 2019, *Mon. Not. Roy. Astron. Soc.*, 485, L83, doi: [10.1093/mnras/slz031](https://doi.org/10.1093/mnras/slz031)

- Rantsiou, E., Burrows, A., Nordhaus, J., & Almgren, A. 2011, *Astrophys. J.*, 732, 57, doi: [10.1088/0004-637X/732/1/57](https://doi.org/10.1088/0004-637X/732/1/57)
- Remillard, R., Morgan, E., Smith, D., & Smith, E. 2000, *IAU Circ.*, 7389, 2
- Rodriguez, C. L., & Antonini, F. 2018, *Astrophys. J.*, 863, 7, doi: [10.3847/1538-4357/aacea4](https://doi.org/10.3847/1538-4357/aacea4)
- Rodriguez, C. L., Zevin, M., Pankow, C., Kalogera, V., & Rasio, F. A. 2016, *Astrophys. J. Lett.*, 832, L2, doi: [10.3847/2041-8205/832/1/L2](https://doi.org/10.3847/2041-8205/832/1/L2)
- Rodriguez, C. L., et al. 2020, *Astrophys. J. Lett.*, 896, L10, doi: [10.3847/2041-8213/ab961d](https://doi.org/10.3847/2041-8213/ab961d)
- Sagert, I., & Schaffner-Bielich, J. 2008, *Astron. Astrophys.*, 489, 281, doi: [10.1051/0004-6361:20078530](https://doi.org/10.1051/0004-6361:20078530)
- Salvesen, G., & Pokawanvit, S. 2020, *Mon. Not. Roy. Astron. Soc.*, 495, 2179, doi: [10.1093/mnras/staa1094](https://doi.org/10.1093/mnras/staa1094)
- Spruit, H., & Phinney, E. S. 1998, *Nature*, 393, 139, doi: [10.1038/30168](https://doi.org/10.1038/30168)
- Stegmann, J., & Antonini, F. 2021, *Phys. Rev. D*, 103, 063007, doi: [10.1103/PhysRevD.103.063007](https://doi.org/10.1103/PhysRevD.103.063007)
- Steinle, N., & Kesden, M. 2021, *Phys. Rev. D*, 103, 063032, doi: [10.1103/PhysRevD.103.063032](https://doi.org/10.1103/PhysRevD.103.063032)
- . 2022, *Phys. Rev. D*, 106, 063028, doi: [10.1103/PhysRevD.106.063028](https://doi.org/10.1103/PhysRevD.106.063028)
- Stevenson, S. 2022, *Astrophys. J. Lett.*, 926, L32, doi: [10.3847/2041-8213/ac5252](https://doi.org/10.3847/2041-8213/ac5252)
- Stevenson, S., Berry, C. P. L., & Mandel, I. 2017, *Mon. Not. Roy. Astron. Soc.*, 471, 2801, doi: [10.1093/mnras/stx1764](https://doi.org/10.1093/mnras/stx1764)
- Stockinger, G., et al. 2020, *Mon. Not. Roy. Astron. Soc.*, 496, 2039, doi: [10.1093/mnras/staa1691](https://doi.org/10.1093/mnras/staa1691)
- Tagawa, H., Haiman, Z., Bartos, I., & Kocsis, B. 2020, *Astrophys. J.*, 899, 26, doi: [10.3847/1538-4357/aba2cc](https://doi.org/10.3847/1538-4357/aba2cc)
- Takahashi, K., & Langer, N. 2021, *Astron. Astrophys.*, 646, A19, doi: [10.1051/0004-6361/202039253](https://doi.org/10.1051/0004-6361/202039253)
- Talbot, C., & Thrane, E. 2017, *Phys. Rev. D*, 96, 023012, doi: [10.1103/PhysRevD.96.023012](https://doi.org/10.1103/PhysRevD.96.023012)
- Tauris, T. M. 2022, *Astrophys. J.*, 938, 66, doi: [10.3847/1538-4357/ac86c8](https://doi.org/10.3847/1538-4357/ac86c8)
- Tiwari, V., Fairhurst, S., & Hannam, M. 2018, *Astrophys. J.*, 868, 140, doi: [10.3847/1538-4357/aae8df](https://doi.org/10.3847/1538-4357/aae8df)
- Vitale, S., Biscoveanu, S., & Talbot, C. 2022, *Astron. Astrophys.*, 668, L2, doi: [10.1051/0004-6361/202245084](https://doi.org/10.1051/0004-6361/202245084)
- Vitale, S., Lynch, R., Sturani, R., & Graff, P. 2017, *Class. Quant. Grav.*, 34, 03LT01, doi: [10.1088/1361-6382/aa552e](https://doi.org/10.1088/1361-6382/aa552e)
- Wang, C., Lai, D., & Han, J. 2006, *Astrophys. J.*, 639, 1007, doi: [10.1086/499397](https://doi.org/10.1086/499397)
- Willems, B., Henninger, M., Levin, T., et al. 2005a, *Astrophys. J.*, 625, 324, doi: [10.1086/429557](https://doi.org/10.1086/429557)
- Willems, B., Kalogera, V., & Henninger, M. 2004, *Astrophys. J.*, 616, 414, doi: [10.1086/424812](https://doi.org/10.1086/424812)
- . 2005b, *ASP Conf. Ser.*, 328, 123. <https://arxiv.org/abs/astro-ph/0404514>
- Wong, T.-W., Willems, B., & Kalogera, V. 2010, *Astrophys. J.*, 721, 1689, doi: [10.1088/0004-637X/721/2/1689](https://doi.org/10.1088/0004-637X/721/2/1689)
- Wongwathanarat, A., Janka, H. T., & Mueller, E. 2013, *Astron. Astrophys.*, 552, A126, doi: [10.1051/0004-6361/201220636](https://doi.org/10.1051/0004-6361/201220636)
- Woosley, S. E. 1987, in *The Origin and Evolution of Neutron Stars*, ed. D. J. Helfand & J. H. Huang, Vol. 125, 255
- Wysocki, D., Gerosa, D., O’Shaughnessy, R., et al. 2018, *Phys. Rev. D*, 97, 043014, doi: [10.1103/PhysRevD.97.043014](https://doi.org/10.1103/PhysRevD.97.043014)
- Yao, J., Zhu, W., Manchester, R. N., et al. 2021, *Nature Astronomy*, 5, 788, doi: [10.1038/s41550-021-01360-w](https://doi.org/10.1038/s41550-021-01360-w)
- Zdziarski, A. A., Veledina, A., Szanecki, M., et al. 2023, *Astrophys. J. Lett.*, 951, L45, doi: [10.3847/2041-8213/ace2c9](https://doi.org/10.3847/2041-8213/ace2c9)
- Zdziarski, A. A., Malyshev, D., Dubus, G., et al. 2018, *Mon. Not. Roy. Astron. Soc.*, 479, 4399, doi: [10.1093/mnras/sty1618](https://doi.org/10.1093/mnras/sty1618)
- Zhang, R. C., Fragione, G., Kimball, C., & Kalogera, V. 2023. <https://arxiv.org/abs/2302.07284>
- Zhu, X.-J. 2021, *Astrophys. J. Lett.*, 920, L20, doi: [10.3847/2041-8213/ac2ba6](https://doi.org/10.3847/2041-8213/ac2ba6)